Journal of Structural Biology 210 (2020) 107493

Contents lists available at ScienceDirect

Journal of Structural Biology

journal homepage: www.elsevier.com/locate/yjsbi

Structure-based design approach to rational site-directed mutagenesis of β-lactoglobulin

Piotr Bonarek[a,1], Joanna I. Loch[b,1], Magdalena Tworzydło[a], David R. Cooper[c], Katažyna Milto[a], Paulina Wróbel[b], Katarzyna Kurpiewska[b], Krzysztof Lewiński[b,*]

[a] Jagiellonian University, Faculty of Biochemistry, Biophysics and Biotechnology, Gronostajowa 7, 30-387 Kraków, Poland
[b] Jagiellonian University, Faculty of Chemistry, Gronostajowa 2, 30-387 Kraków, Poland
[c] University of Virginia, Department of Molecular Physiology and Biological Physics, 1340 Jefferson Park Avenue, Charlottesville, VA 22908, USA

ARTICLE INFO

Keywords:
Lipocalin
Lactoglobulin
Protein engineering
Mutagenesis
Binding pocket geometry
Anticalin proteins

ABSTRACT

Recombinant proteins play an important role in medicine and have diverse applications in industrial biotechnology. Lactoglobulin has shown great potential for use in targeted drug delivery and body fluid detoxification because of its ability to bind a variety of molecules. In order to modify the biophysical properties of β-lactoglobulin, a series of single-site mutations were designed using a structure-based approach. A 3-dimensional structure alignment of homologous molecules led to the design of nine β-lactoglobulin variants with mutations introduced in the binding pocket region. Seven stable and correctly folded variants (L39Y, I56F, L58F, V92F, V92Y, F105L, M107L) were thoroughly characterized by fluorescence, circular dichroism, isothermal titration calorimetry, size-exclusion chromatography, and X-ray structural investigations. The effects of the amino acid substitutions were observed as slight rearrangements of the binding pocket geometry, but they also significantly influenced the global properties of the protein. Most of the mutations increased the thermal/chemical stability without altering the dimerization constant or pH-dependent conformational behavior. The crystal structures reveal that the I56F and F105L mutations reduced the depth of the binding pocket, which is advantageous since it can reduce the affinity to endogenous fatty acids. The F105L mutant created a unique binding mode for a fatty acid, supporting the idea that lactoglobulin can be altered to bind unique molecules. Selected variants possessing a unique combination of their individual properties can be used for further, more advanced mutagenesis, and the presented results support further research using β-lactoglobulin as a therapeutic delivery agent or a blood detoxifying molecule.

1. Introduction

Recombinant proteins are a growing group of innovative therapeutic agents with applications in various medical disciplines. This group of biopharmaceuticals is diverse and includes hormones, cytokines, growth factors, plasma proteins, enzymes, inhibitors, coagulation factors, fusion proteins, antigen-binding fragments (Fab), antibody-drug conjugates, and monoclonal antibodies (Lagassé et al., 2017; Shepard et al., 2017). Antibodies are currently one of the most promising therapeutic agents but have several disadvantages; therefore, alternatives to antibodies are intensively being developed. Among them are Anticalins, a novel class of engineered human lipocalins with increased affinities to selected biological targets (Rothe and Skerra, 2018). Anticalins have many advantages over classical therapeutic antibodies; they are relatively small with a compact β-barrel fold and have a high structural stability, high target specificity, low immunogenicity, and low cost of production in *E. coli* cells (Gebauer and Skerra, 2012; Richter et al., 2014). The high specificity of Anticalins to selected targets is achieved by combinatorial design with the use of targeted random mutagenesis and phage display selection (Skerra, 2013). Mutations are introduced to the region of flexible loops allowing the substituted residues to interact specifically with molecular targets such as receptors (Richter and Skerra, 2017) (Anderson et al., 2015), peptides (Gille et al., 2016; Hohlbaum et al., 2018), or small molecules (Barkovskiy et al., 2019; Dauner and Skerra, 2019; Eggenstein et al., 2014).

β-Lactoglobulin (BLG) is a widely-studied lipocalin present in bovine milk and has a recognized potential for use as a potential

* Corresponding author.
E-mail address: lewinski@chemia.uj.edu.pl (K. Lewiński).
[1] These authors contributed equally to this work.

https://doi.org/10.1016/j.jsb.2020.107493
Received 19 July 2019; Received in revised form 6 March 2020; Accepted 9 March 2020
Available online 10 March 2020

molecular transporter of therapeutic agents (Bijari et al., 2019; Shafaei et al., 2017; Wilde et al., 2016). Furthermore, recent advances suggest that lipocalins can serve as potential toxin remover (Jenkins et al., 2019; Rudra et al., 2018) and be used in potentially life-saving extracorporeal dialysis systems for individuals suffering from impaired kidney function or a drug overdose (Tumlin, 2019). The ability of BLG to specifically bind to chemotherapeutic drugs, such as oxali-palladium and 5-fluorouracil (Leilabadi-Asl et al., 2018), and its ability to form nanoparticles make it an attractive delivery system for therapeutic agents (Ghalandari et al., 2014). Recently, BLG nanoparticles loaded with folic acid and doxorubicin showed great promise to serve as a receptor-mediated drug delivery system for use against breast cancer (Kayani et al., 2018). BLG has a natural affinity to a wide range of hydrophobic ligands (e.g., fatty acids and carotenoids) (Liu et al., 2018; Loch et al., 2012), medicines (Shahraki and Shiri, 2018), and others (Sawyer, 2013) and has therefore been extensively studied as a potential drug carrier. However, the therapeutic use of the animal-originated lactoglobulin is currently limited due to its immunogenicity in humans (Kurpiewska et al., 2019). Recently, several ways of BLG modification have been proposed to reduce its allergenicity, e.g., covalent conjugation with dietary polyphenols (Wu et al., 2018) or the introduction of a mutation in the region of lactoglobulin epitopes (Kazem-Farzandi et al., 2015; Taheri-Kafrani et al., 2015). Lactoglobulin mutagenesis has not only been performed to decrease its immunogenicity, but single mutations have been introduced to improve secretion of recombinant BLG from expression host *P. pastoris* (Katakura et al., 1999), to investigate the effect of mutations on protein dimerization (Sakurai and Goto, 2002) and aggregation (Jayat et al., 2004), and to modify BLG thermal and chemical stability (Cho et al., 1994; Jayat et al., 2004; Yagi et al., 2003; Zhao and Feng, 2018). However, mutagenesis has never been performed in the region of lactoglobulin's binding pocket, so there is no information on how individual substitutions inside the β-barrel would influence ligand binding and protein stability. Such data are extremely important for designing BLG therapeutic variants with an optimal structural stability and high ligand affinity. In order to modify the binding properties of β-lactoglobulin, we started a systematic study of new BLG variants with mutations in the binding pocket region.

The aim of our study was to design new lactoglobulin variants with single-site mutations inside the β-barrel and to evaluate them in terms of their suitability for further modifications and applications. We evaluated how these substitutions affect dimerization, resistance to denaturing agents (high temperature, urea), pH-dependent conformational behavior, affinity to natural ligands (fatty acids), and the geometry of the binding pocket. It was particularly important to identify stable and soluble variants with a reduced depth of the binding pocket. Such mutants should have reduced affinity to aliphatic chains, thereby preventing non-specific binding of fatty acids and their derivatives from body fluids. As the far-reaching goal of the study is to produce medically useful lactoglobulin variants, such a property is highly desirable. Single-site mutants with promising biophysical properties will be prerequisites to advanced mutagenesis leading to the production of BLG variants for which altered size and shape of the binding pocket would determine affinities to selected classes of compounds.

The location of single-site mutations were selected on the basis of protein–ligand interactions analysis of the previously determined lactoglobulin crystal structures. The type of amino acid substitutions were selected using a structure-based approach utilizing 3-dimensional (3D) alignment of proteins with almost identical fold but low sequence identity. Newly obtained BLG variants were produced in *E. coli,* purified, and characterized using various experimental techniques: fluorescence and circular dichroism measurements, isothermal titration calorimetry, size-exclusion chromatography, and X-ray crystallography.

2. Materials and methods

2.1. Design of new BLG variants

In the first step of designing new variants, the potential mutation positions in the β-barrel were selected based on previously determined crystal structures of lactoglobulin complexes (Loch et al., 2011, 2012, 2013b, 2015a). The residues L39, V43, I56, L58, V92, F105, M107, and L122 located inside the binding pocket were found to be the most suitable for site-directed mutagenesis. To select the type of substitution, a search for proteins of the mammalian origin possessing high structural similarity to bovine β-lactoglobulin was made in the Protein Data Bank using the jFATCAT-rigid algorithm (Prlic et al., 2010). Eight proteins of relatively low sequence similarity were selected for final analysis: *bovine lipocalin allergen Bos d 2* (PDB ID: 1BJ7), *major horse allergen Equ c 1* (PDB ID: 1EW3), *mouse major urinary protein 1* (PDB ID: 1QY0), *mouse major urinary protein 6* (PDB ID: 2NND), *possum milk whey lipocalin* (PDB ID: 2R74), *mouse major urinary protein 2* (PDB ID: 2OZQ), *mouse major urinary protein 4* (PDB ID: 3KFF) and *dog lipocalin allergen Can f 2* (PDB ID: 3L4R). The selected proteins had sequence similarity in the range 37.8% − 45.1% (*EMBOSS Needles Global* alignment tool) (Needleman and Wunsch, 1970) and were superimposed in *PyMol* (command: align) with resulting RMSD values in the range of 1.04–3.22 Å (Fig. S1).

2.2. Site-directed mutagenesis, protein expression and purification

The bovine β-lactoglobulin gene was cloned to the pETDuet-1 expression vector also carrying a DsbC gene, so all new BLG variants were co-expressed with the prokaryotic disulfide bond isomerase DsbC. Expression was performed in *E. coli Origami B (DE3)* strain according to a previously published protocol (Loch et al., 2016). All new variants are derivatives of recombinant WT β-lactoglobulin (isoform B) carrying two N-terminal mutations L1A and I2S, which facilitate cleavage of the starting Met (Loch et al., 2016). Single-site mutations: L39Y, V43Y, I56F, L58F, V92F, V92Y, F105L, M107L, and L122Y, were introduced to the protein sequence using the *QuickChange* protocol (Xia et al., 2015). WT protein and all mutants were purified according to protocol #2 (Loch et al., 2016) which included ion-exchange chromatography using *Fractogel TMAE (S)* (Merck Millipore) and gel filtration using *Superdex G75* (GE Healthcare). Protein purity and homogeneity were checked by SDS-PAGE. The efficiency of purification depended on the mutant and varied from 20 to 60 mg of protein per 1L of bacterial liquid culture. The obtained proteins were used for crystallization with no additional purification steps. Prior to the fluorescence, CD, and ITC measurements, proteins were additionally purified by ion-exchange chromatography on a *MonoQ* HR10/10 column (GE Healthcare). A 50 mM phosphate buffer at pH 6.5 with a linear gradient (0–350 mM) of NaCl and a flow-rate of 4 ml/min was used to elute the bound protein from the column. The fractions containing BLG were collected and stored at −20 °C.

2.3. Circular dichroism: far-UV, near-UV and pH-dependent measurements

CD spectra were recorded at 20 °C on a JASCO J-710 spectropolarimeter using 5 or 50 mM phosphate buffer pH 6.5. Protein concentrations of 200 nM and a 2 cm path length were used for far-UV measurements, while 20–70 μM protein concentrations and a 5 mm path length were used for near-UV measurements. At least three scanning acquisitions were accumulated and averaged to yield the final spectrum. CD spectra were corrected for the buffer baseline. The recorded ellipticity was re-calculated to $\Delta\varepsilon$ to compensate for the difference in extinction coefficients. Spectra were normalized to the peptide bond concentration for far-UV and the protein concentration for near-UV. The BLG concentration was determined spectrophotometrically at 278 nm using absorption coefficient $\varepsilon = 18800\ M^{-1}cm^{-1}$ for L39Y and V92Y variants and $17600\ M^{-1}cm^{-1}$ for the rest of mutants (Loch et al.,

2016).

The pH-dependent measurements were conducted at a constant protein concentration (5 μM) at pH from 4 to 10 (with an interval of 0.5). Thirteen buffer solutions of different pH were prepared according to Britton and Robinson (Britton and Robinson, 1931). A mixture containing 25 mM boric acid, 25 mM acetate sodium, and 25 mM phosphate sodium (BAP) was divided into thirteen solutions. The obtained mixtures were adjusted to the appropriate pH with 5 M HCl or 5 M NaOH. Before measurements, samples were incubated at least 30 min at room temperature.

2.4. Fluorescence: Competitive binding assay and pH-dependent measurements

The fluorescence measurements were conducted in 50 mM Tris-HCl buffer pH 8.0 at 25 °C using a *Fluorolog3* spectrofluorimeter (Horiba, France). 2 ml of 5 μM protein was mixed with 6 μM ANS (8-anilino-1-naphthalenesulfonic acid) solution freshly prepared just before measurement, and the mixture was titrated with 1 mM ethanolic solution of palmitic acid up to at least 1.5 fold excess of the ligand. The final concentration of ethanol did not exceed 1% (v/v) of the sample volume. The experiments were done in duplicates. The fluorescence emission spectra were recorded in range 360–600 nm with excitation at 350 nm. The range of 515–600 nm was integrated for every spectrum and analyzed according to the one site binding model to determine the apparent value of the binding constant (K_{app}) and stoichiometry (n_{app}). Fluorescence measurements at pH from 4 to 10 (protein samples prepared as described in CD section) were conducted using quartz cuvette with 3 × 3 mm path length with an excitation 295 nm end emission 305–400 nm. Each spectrum was averaged from 3 independent acquisitions and the buffer signal was subtracted before analysis.

2.5. Thermal and chemical denaturation

Thermal unfolding of the protein was monitored by CD signal and was measured on a JASCO J-710 spectropolarimeter using a 1 mm path-length quartz cuvette in 50 mM phosphate buffer pH 6.5, for protein concentration of 10–12 μM, according to the method described previously (Loch et al., 2016).

Urea-induced unfolding was monitored by CD and tryptophan fluorescence. The measurements were done in 50 mM phosphate buffer pH 6.5 at room temperature. The samples were prepared one day before the experiment by mixing a stock solution of the protein with 10 M urea in the same buffer to the final BLG concentration 5 μM and incubated overnight at room temperature. The CD signal at 220 nm was measured on a JASCO J-710 spectropolarimeter using a 1 mm path-length quartz cuvette. Global analysis of data in triplicates was conducted using Origin software assuming a two-state mechanism according to methods described by D'Alfonso (D'Alfonso et al., 2002).

Fluorescence measurements were conducted using quartz cuvette with a 3 × 3 mm path length with an excitation at 295 nm and emission at 305–400 nm. The buffer signal was subtracted before analysis. The analysis was performed according to the method proposed by Laptenok et al., (2011) and van Stokkum and Laptenok (2014). The fluorescence spectra of folded and unfolded protein were modeled as a skewed Gaussian in the energy domain ($\bar{\nu} = 1/\lambda$) and were described by three parameters: peak location $\bar{\nu}_{max}$, width $\Delta\bar{\nu}$, and skewness b. All spectra were globally analyzed as a linear combination of native and unfolded protein spectra. The fraction of the native form was calculated according to the two-state denaturation model assuming the linear dependence of spectra intensity from urea concentration. The analysis was done for the data collected from three independent experiments and the average values with standard deviation are presented as a result.

2.6. Isothermal titration calorimetry

All ITC experiments were carried out at 25 °C using a VP-ITC instrument (MicroCal, Northampton, MA, USA). The protein was concentrated to 450–600 μM in 50 mM phosphate buffer pH 6.5 and titrated into the cell loaded with a buffer solution. Typically, 20–25 additions of 8 μL of a high protein concentration solution were made. Both solutions were degassed before experiments and a constant stirring speed of 300 rpm was maintained during the experiment. Data analysis was performed using MicroCal Origin scientific plotting software according to the simple dimer dissociation model described in details elsewhere (Bello et al., 2008).

2.7. Size-exclusion chromatography

The experiments were performed in triplicates using a *Superdex200 Increase* chromatographic column (GE Healthcare) with a flow rate of 1 ml/min in phosphate buffer pH 6.5 at room temperature. The absorption at 220 and 280 nm was recorded. The elution volume of the protein (V_e) was calculated in Origin software using the built-in peak analyzer function. The partition coefficient was calculated according to the equation:

$$K_{av} = (V_e - V_0)/(V_C - V_0)$$

where V_0 is the column interstitial volume and V_C is the total volume of the column packing. V_0 was determined as elution of Blue dextran (MW about 2 000 000 Da), while V_C was calculated from the geometric dimensions of the column.

2.8. Crystallization

Prior to crystallization, proteins were concentrated to 10–40 mg/ml using *Amicon Ultra Centrifugal Filters* with 10 kDa cut-off membrane (EMD Millipore). Correctly folded and stable BLG mutants (L39Y, I56F, L58F, V92F, V92Y, F105L, and M107L) were crystallized by the vapor diffusion method in hanging drop setup. Additionally, recombinant WT (Wild Type) lactoglobulin was crystallized in order to obtain crystals of trigonal symmetry, the same symmetry as determined for most of the mutants used in this study. Diffraction quality crystals of individual mutants were obtained from 2.4 − 3.0 M ammonium sulfate or 1.34 M sodium citrate in 0.1 M Tris-HCl pH 7.1–8.0. See Table S1 for details. In each experiment, 500 μL of crystallization solution was placed inside the crystallization plate well.

Mutants F105L and M107L crystallized in an orthorhombic form, but these crystals poorly diffracted X-rays. In order to obtain better diffracting crystals, we decided to co-crystallize mutants F105L and M107L with a fatty acid. Although lactoglobulin has the highest affinity [μM] to 16-carbon palmitic acid (PLM) (Loch et al., 2012), the 14-carbon myristic acid (MYR) was used because it has higher water solubility than PLM and, unlike PLM, does not form a strong precipitate in the drop which disturbs the lactoglobulin crystallization process. This strategy was successful for F105L and M107L mutants, but no significant improvement of diffraction was observed upon co-crystallization of L58F with MYR. Variant I56F did not crystallize in the presence of MYR, therefore the shorter, 12-carbon lauric acid was used. The addition of lauric acid facilitated growing of I56F crystals; however, the crystal structure revealed that no ligand was bound. Crystallization experiments at conditions used for other mutants did not produce crystals of V92F and V92Y variants.

2.9. X-ray data collection and structure refinement

X-ray diffraction data were collected on *SuperNova* (Rigaku Oxford Diffraction) diffractometer equipped with a 135 mm Atlas CCD detector and microfocus X-ray source (1.54 Å) operating at 50 kV and 0.8 mA. Due to the small size of the crystals of the unliganded form of M107L

Table 1
Statistics of data collection and structure refinement.

Mutant	WT	L39Y-(PLM)	I56F	L58F	F105L	M107L	L58F-MYR	F105L-MYR	M107L-MYR
	no ligand additive						ligand additive (co-crystallization)		
Ligand	no	yes	no	no	no	no	yes	yes	yes
type of ligand	–	$PLM^{endogenous}$	–	–	–	–	$MYR^{co\text{-}cryst}$	$MYR^{co\text{-}cryst}$	$MYR^{co\text{-}cryst}$
PDB ID	6QI6	6QI7	6QPD	6QPE	6XVE	6RYT	6RWP	6RWQ	6RWR
space group	$P3_221$	$P3_221$	$P3_221$	$P3_221$	$C222_1$	$P22_12_1$	$P3_221$	$P3_221$	$P3_221$
Unit cell: a, b, c [Å]	52.73, 52.73, 110.33	53.31, 53.31, 110.42	53.27, 53.27, 113.05	52.67, 52.67, 112.01	54.74, 79.77, 66.09	56.16, 61.52, 78.24	53.08, 53.08, 111.56	53.07, 53.07, 112.13	53.18, 53.18, 112.29
Resolution range	14.07–2.00 (2.05–2.00)	14.75–2.50 (2.61–2.50)	13.81–2.00 (2.05–2.00)	13.68–2.20 (2.27–2.20)	14.49–2.15 (2.22–2.15)	48.41–2.10 (2.16–2.10)	14.78–2.10 (2.17–2.10)	14.18–2.05 (2.11–2.05)	13.47–2.10 (2.16–2.10)
Completeness [%]	99.2 (97.8)	99.4 (100.0)	98.5 (96.4)	98.3 (93.9)	98.6 (98.2)	93.1 (95.6)	99.3 (98.9)	99.5 (99.6)	99.1 (97.2)
No. of reflections	31 832	21 453	31 623	26 229	16 628	49 058	31 724	31 794	29 317
No. of unique reflections	12 441	6 635	12 897	9 457	7 984	15 140	11 062	11 972	11 138
Mean I/σ(I)	9.5 (1.8)	9.0 (2.0)	7.4 (1.7)	6.8 (2.3)	16.6 (2.0)	4.7 (2.0)	10.6 (2.0)	6.6 (2.2)	10.9 (1.8)
CC(1/2)	0.998 (0.681)	0.997 (0.845)	0.993 (0.596)	0.990 (0.878)	0.999 (0.895)	0.989 (0.846)	0.997 (0.761)	0.990 (0.905)	0.998 (0.651)
Redundancy	2.6 (1.9)	3.2 (2.8)	2.5 (2.0)	2.8 (1.8)	2.1 (1.5)	3.2 (3.2)	2.9 (2.1)	2.7 (2.0)	2.6 (1.9)
R_{merge}	0.049 (0.405)	0.062 (0.393)	0.088 (0.446)	0.085 (0.183)	0.031 (0.253)	0.100 (0.471)	0.059 (0.355)	0.084 (0.215)	0.057 (0.446)
R_{work}/R_{free} (%)	18.6/24.6	19.5/26.2	20.7/26.9	18.5/25.1	23.0/29.1	21.4/27.8	19.4/24.5	19.1/25.5	17.4/22.1
Bond lengths RMSD (Å)	0.010	0.008	0.010	0.010	0.008	0.009	0.008	0.010	0.009
Bond angles RMSD (°)	1.628	1.505	1.362	1.362	1.546	1.598	1.547	1.358	1.315
Ramachandran outliers (%)	0	0	0	0	0	0	0	0	0
Ramachandran favored (%)	97	98	96	95	94	96	97	98	97
Ramachandran allowed (%)	3	2	4	5	6	4	3	2	3
Total no. of protein atoms	1208	1171	1257	1234	1021	1125	1160	1204	1225
Average B value for all protein atoms ($Å^2$)	41.12	48.92	27.54	26.10	39.15	40.44	31.08	35.91	35.40

crystals, diffraction data were collected at beamline P13 MX1 at PETRA III (EMBL/DESY, Hamburg, Germany). All data were collected at 100–120 K. Prior to data collection, crystals were immersed for a few seconds in mother liquor solution containing 15–20% (v/v) of glycerol or ethylene glycol. X-ray diffraction data were processed using $Crysalis^{Pro}$ (Rigaku Oxford Diffraction) or XDS (Kabsch, 2010) and scaled using Aimless (Evans and Murshudov, 2013) from the CCP4 package (Winn et al., 2011). Structures were solved by molecular replacement in Phaser (Read et al., 2013) and refined in Refmac5 (Murshudov et al., 2011), electron density maps were investigated in Coot (Winn et al., 2011). Statistics of data collection and structure refinement are summarized in Table 1. Structures were deposited in PDB as entries: 6QI6, 6QI7, 6QPD, 6QPE, 6RYT, 6RWP, 6RWQ, 6RWR and 6XVE (Table 1).

3. Results

3.1. Design of new lactoglobulin variants

Various computational techniques can be used to predict the influence of mutations on protein structure (Frappier et al., 2015; Pandurangan et al., 2017; Pires et al., 2014). As they often give inconsistent predictions, we have used a different approach to identify residues suitable for substitutions that can potentially change the geometry of the binding site without affecting protein stability. The residues L39, V43, I56, L58, V92, F105, M107, and L122 were selected because of their specific location in the β-barrel. L39 located on the AB loop occupies a position at the binding pocket entrance and its side chain fills the space between loops AB and GH, close to EF and GH loops involved in Tanford transition (Sakurai and Goto, 2006). L58 and M107 are located in the upper part of the binding pocket, while I56, V92, F105, V43, and L122 occupy a position in the middle part of the binding pocket (Fig. 1 and Fig. S1). In most of the known BLG-ligand complexes the selected residues are involved in interactions with hydrophobic compounds.

To decide which amino acids are the most promising alternatives to the natural residues, we considered several of their properties, namely hydrophobicity, ability to form specific interactions with ligands, potential influence on the binding pocket geometry, and the potential stabilizing effect of substitution resulting from the van der Walls interactions to neighboring residues. It has been previously observed that lactoglobulin can spontaneously bind natural fatty acids from the expression host under certain conditions (Loch et al., 2016). When this happens, the binding pocket is blocked by a tightly bound fatty acid that prevents the binding of target molecules. Therefore, it was important to shorten the naturally elongated binding pocket in order to reduce the protein's affinity to fatty acids.

To evaluate whether a highly hydrophobic binding pocket would tolerate any polar substitutions, three BLG mutants were produced: V43N, I56Q, and V92Q. These mutations had a detrimental effect on protein folding and stability suggesting that the β-barrel interior can accept only non-polar substitutions. To find out what types of amino acids can be tolerated in particular positions, the structural comparison of BLG and other lipocalins found in the PDB (Table S2) has been performed according to the procedure described in the Materials and Methods section. The comparison revealed that some hydrophobic residues in BLG can be substituted by aromatic or aliphatic amino acids. Finally, nine variants were designed and produced: L39Y, V43Y, I56F, L58F, V92F, V92Y, F105L, M107L, and L122Y. The substitutions V43Y and L122Y resulted in expression of insoluble protein forming inclusion bodies, thus these variants were rejected from further investigations. For comparison to the mutant V92F, a similar variant V92Y was designed to test whether the polar hydroxyl group would affect protein stability and ligand binding specificity. Also, L39 was replaced by tyrosine, not by phenylalanine, as suggested by the results of the analysis, because the binding site entrance is more polar than the β-barrel

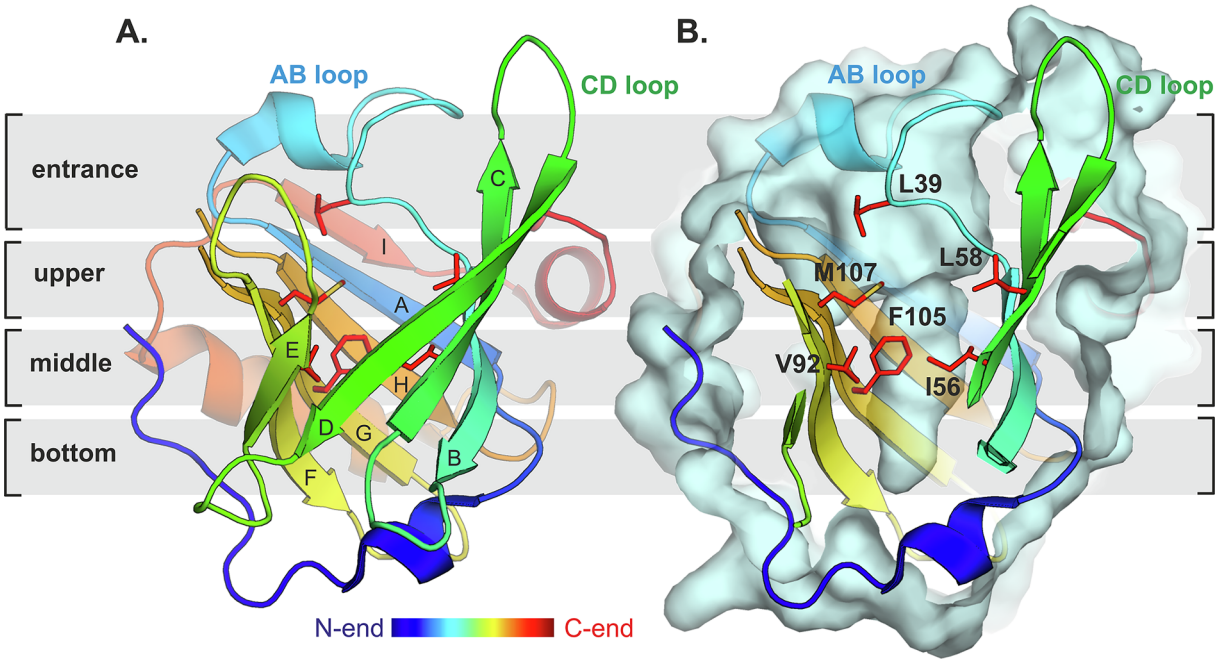

Fig. 1. (**A**) Overall WT lactoglobulin structure with marked β-strands A-I and terms used for description of the binding pocket depth (from entrance to bottom). Residues selected for mutagenesis that resulted in production of correctly folded mutants are marked in red; their location in the binding pocket is shown in the cartoon and (**B**) in cut-away representation showing the elongated shape of WT binding pocket. Solvent-accessible surface was drawn using probe radius 1.4 Å.

interior. Further experiments showed that our concept of mutagenesis was effective and we were able to efficiently produce and characterize seven correctly folded lactoglobulin variants.

3.2. Protein dimerization

Previous studies have demonstrated the importance of BLG dimerization for the protein structural stability and its affinity to ligands (de Wit, 2009; Gutiérrez-Magdaleno et al., 2013; Qi et al., 1995). Therefore, we decided to determine the impact of mutations on the BLG dimerization process using dilution experiments using ITC. The previous calorimetric investigations of BLG isoforms A and B revealed a slight uptake of protons accompanying dimerization with ΔN_{H+} equal to 0.21 and 0.24, respectively (Bello et al., 2011, 2008). To minimize the buffer ionization contribution, the dimerization constants for all mutants and recombinant WT protein were determined in phosphate buffer. The thermodynamic parameters of dimerization are summarized in Table 2. Both ΔG_{dim} and its contributions ΔH_{dim} and ΔS_{dim} determined for recombinant WT are comparable with previous calorimetric results obtained for BLG-A (isoform A) and BLG-B (isoform B) at pH 7.0 (Bello et al., 2011, 2008), and for BLG-B and goat lactoglobulin at pH 7.5 (Loch et al., 2015b).

Despite the fact that all mutations are located in an area distant from the dimer interface, for some variants, the substitutions influenced the dimerization process. In comparison to WT, the most significant increase of K_{dim} was observed for variants L58F and V92F (2- and 2.4-fold, respectively), while for L39Y and F105L, a drop by more than half was observed. In all cases, the dimerization is mostly enthalpy driven process, except F105L for which the entropic component contributes more significantly to ΔG_{dim}.

The largest difference in ΔG_{dim} was between V92F and F105L. For these variants the $\Delta\Delta G_{dim}$ was 5 kJ/mol while $\Delta\Delta H_{dim}$ was nearly 12 kJ/mol. The linear dependence of ΔH_{dim} from ΔS_{dim} presented in Fig. 2A, characterized by $R^2 = 0.93$ and its slope equal to 440, showed that enthalpy–entropy compensation occurred and was the result of a specific chemical process, not a measurement artifact (Krug et al., 1976). The exception is mutant L39Y, which significantly deviates from the trend. This substitution is also the only one which resulted in unfavorable change of entropy. Since none of the mutations affect residues that create the dimer interface, changes in K_{dim} might be the result of fluctuations in other regions of the protein chain.

To further characterize the effect of the single-site mutations on the quaternary structure, size exclusion chromatography was performed using *Superdex 200 Increase* column at pH 6.5. A single peak of identical shape was observed for all variants (see inset in Fig. 2B) and the observed retention times were consistent with the molecular weight of the dimer. The elution volumes ranged from 15.00 to 15.28 ml (Fig. 2B). The presence of only one peak on chromatograms indicates the lack of a tendency for variants to form higher-order oligomers. The peak shape is consistent with the reversible dimerization typical for BLG and indicates fast association and slow dissociation that leads to the appearance of a characteristic tailing (Yu et al., 2006). In such a case, the position of elution maximum depends on the average value of the partition coefficient K_{av} of monomeric and dimeric forms. Since all experiments were carried out using the same column and at the same protein concentration, the peak elution volume should be proportional to K_{dim}. For all variants except L39Y and F105L, the observed K_{av} vs K_{dim} relationship is linear with R^2 0.97 (Fig. 2B). This means that the hydrodynamic volume was the same for these mutants and observed differences in elution volume were merely the result of different dimer-monomer equilibrium. Mutants L39Y and F105L did not follow this

Table 2
Thermodynamic parameters of BLG mutants dimerization in phosphate buffer, pH 6.5 at 25 °C.

	K_{dim} ($\times 10^3$ M^{-1})	ΔG_{dim} (kJ/mol)	ΔH_{dim} (kJ/mol)	$-T\,\Delta S_{dim}$ (kJ/mol)
WT	56 ± 17	−27.1 ± 0.7	–22.4 ± 2.1	−4.7 ± 2.2
L39Y	25 ± 4	−25.1 ± 0.4	−25.5 ± 1.0	0.4 ± 1.1
I56F	54 ± 18	−27.0 ± 0.8	−18.4 ± 1.9	−8.6 ± 2.1
L58F	111 ± 41	−28.8 ± 0.9	−25.3 ± 4.0	−3.5 ± 4.1
V92F	135 ± 54	−29.3 ± 1.0	−26.2 ± 6.1	−3.1 ± 6.2
V92Y	60 ± 16	−27.3 ± 0.7	−25.4 ± 1.9	−1.9 ± 2.0
F105L	18 ± 3	−24.2 ± 0.5	−14.3 ± 0.5	−10.0 ± 0.7
M107L	69 ± 19	−27.6 ± 0.7	−19.9 ± 2.1	−7.7 ± 2.2

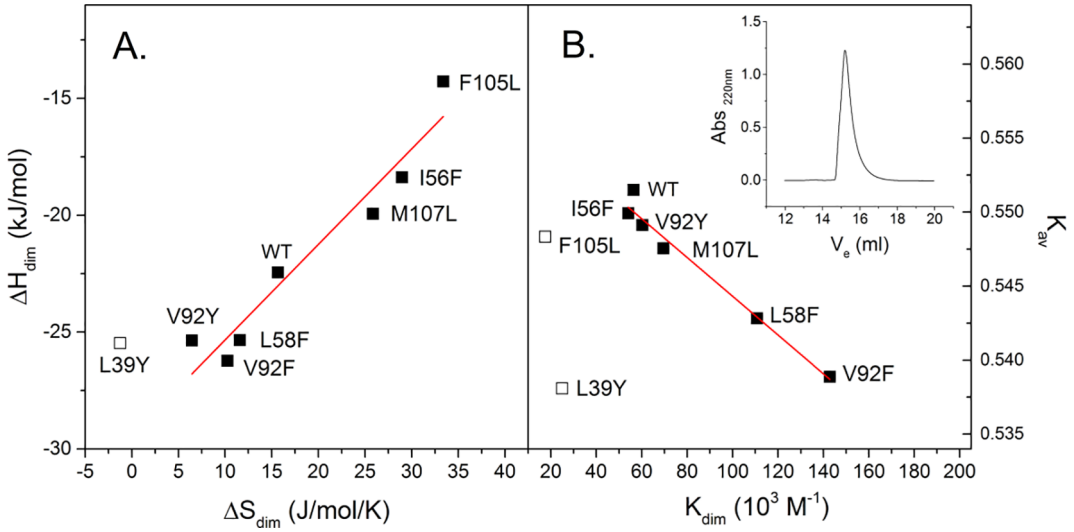

Fig. 2. (A) The enthalpy–entropy compensation during BLG mutants' dimerization in phosphate buffer pH 6.5 at 25 °C. Each value is the result of the analysis three independent measurements. Mutant L39Y has been excluded during linear regression analysis (red line). **(B)** The dependence of hydrodynamic parameter (K_e) vs dimerization constant (K_{dim}) of the protein. The linear dependence is observed for all proteins except L39Y and F105L (R^2 = 0.97). Inset: SEC chromatogram of I56F performed using *Superdex 200 Increase* column with phosphate buffer pH 6.5 and flow rate of 0.5 ml/min.

trend and their elution volumes were lower than expected.

3.3. Secondary and tertiary protein structure in solution

Circular dichroism was used to determine whether substitutions affect the secondary and tertiary structure of lactoglobulin in solution. As the quaternary structure can affect the CD spectra in far-UV, all measurements were made using a 200 nM protein solution. In such conditions, more than 95% of the protein molecules are monomeric and thus the changes in CD signal can be interpreted as the result of substitution only. Spectra are presented in Fig. 3 and the secondary structure content is summarized in Table S3.

CD spectra revealed that secondary structure has been well preserved in all new variants and were in good agreement with values determined previously for protein isolated from milk (Creamer et al., 1983). The largest changes were observed for helix content in L39Y, I56F (−5%) and V92Y (+4%). The content of the β-sheet, unordered structure, and turns are in the range of 34–40%, 26–30%, and 21–24%, respectively.

The CD signal recorded in near UV originates from the absorption of aromatic residues and cystines and enables monitoring of changes in the tertiary structure. Previous analysis of lactoglobulin CD spectra in this region indicated that dimerization at neutral pH is not accompanied by significant changes in the tertiary structure (Bello et al., 2008). Therefore, experiments could be performed at higher protein concentrations (20–70 μM) to gain a better signal to noise ratio. Recorded spectra normalized to BLG concentration are presented in Fig. 3B.

Analysis of near-UV spectra showed that they are comparable with each other and with spectrum previously recorded for the WT protein. The positions of all the extremes observed for WT lactoglobulin are preserved, in particular, minima at 293 and 286 nm, which only changed in intensity. This indicates that the introduction of additional aromatic residues does not significantly contribute to the measured CD signal. In our previous work, such changes were interpreted as an effect of the protein dynamics related deviations around W19 located deep in

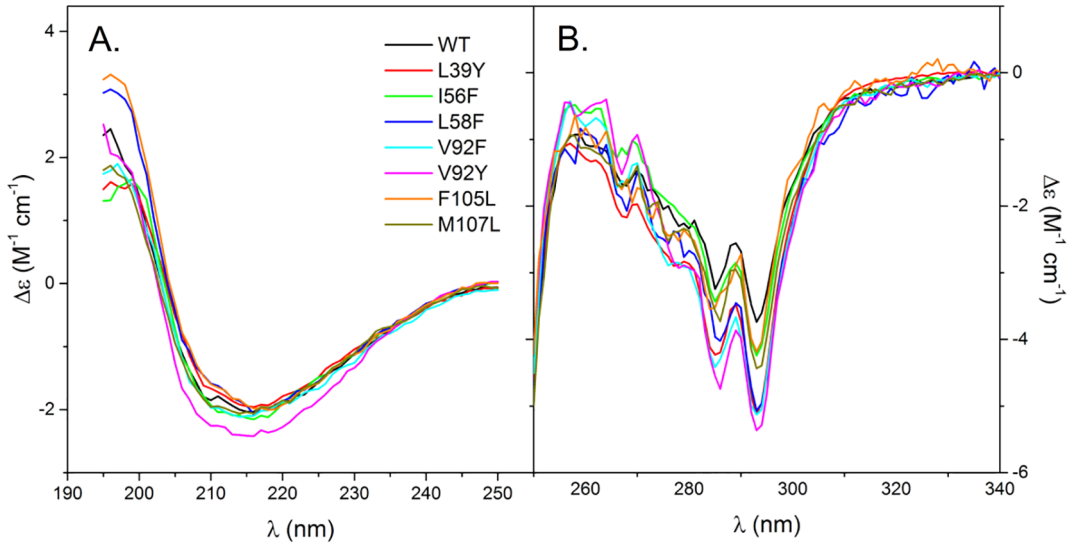

Fig. 3. CD spectra in far UV for 200 nM proteins (A) and in near UV for 20–70 μM proteins (B) in 50 mM phosphate buffer pH 6.5 at room temperature. Spectra of WT comes from (Loch et al., 2016).

Table 3
Chemical denaturation parameters and temperatures of thermal denaturation transition of BLG mutants determined in phosphate buffer, pH 6.5.

	Fluorescence			Circular dichroism			T_m (°C)
	ΔG^0_{fluo} (kJ/mol)	m_{fluo} (kJ/mol/M)	$[urea]_{1/2}$	ΔG^0_{CD} (kJ/mol)	m_{CD}(kJ/mol/M)	$[urea]_{1/2}$	
WT	18.3 ± 2.6	4.7 ± 0.5	3.9	16.2 ± 2.4 [a]	3.9 ± 0.6 [a]	4.2 [a]	77.5
L39Y	30.3 ± 3.0	6.2 ± 0.5	4.9	40.2 ± 9.9	8.0 ± 2.0	5.0	82.1
I56F	33.5 ± 3.5	6.4 ± 0.5	5.2	37.1 ± 9.7	7.1 ± 1.9	5.3	71.0
L58F	27.3 ± 1.1	6.3 ± 0.3	4.4	28.2 ± 4.6	6.2 ± 1.0	4.5	83.0
V92F	22.8 ± 0.3	4.9 ± 0.1	4.6	30.5 ± 5.0	6.6 ± 1.1	4.6	76.2
V92Y	17.2 ± 1.2	5.0 ± 0.3	3.4	16.7 ± 2.3	4.6 ± 0.6	3.6	64.7
F105L	24.8 ± 2.8	6.0 ± 0.3	4.2	25.0 ± 9.4	5.6 ± 2.1	4.5	82.8
M107L	23.0 ± 0.8	5.3 ± 0.1	4.4	17.7 ± 2.6	4.3 ± 0.6	4.2	81.5

[a] values from (Loch et al., 2016)

the hydrophobic pocket (Loch et al., 2015b). According to such criterion, we can divide mutants into two groups: those variants with dynamics similar to WT (I56F, F105L, and M107L) and those possessing a more rigid structure near W19 (L39Y, L58F, V92F, V92Y).

3.4. Chemical and thermal stability

Chemical and thermal denaturation methods were used to determine the effect of mutations on lactoglobulin stability. For chemical denaturation experiments, urea was chosen as a chemical denaturant, and the process was monitored by changes in the tryptophan fluorescence (Fig. S2) and changes of the CD signal at 220 nm. In both cases, the analysis was possible using a simple two-state model. The high similarity of fluorescence spectra of all variants after denaturation is presented in Fig. S2 and it indicates a similar degree of unfolding of all proteins. The shift of λ_{max} from 328 nm for the native state to 345 nm for the denatured and solvent-exposed state is consistent with the results of previous studies (D'Alfonso et al., 2002). The values of protein stability parameters, ΔG^0, m and $[urea]_{1/2}$, determined by both methods are summarized in Table 3. The observed discrepancies in ΔG^0 determined by both methods for some variants may be related to the presence of transition states during the denaturation of lactoglobulin. The analysis showed increased chemical stability for all variants, except for V92Y and M107L. The highest urea-resistance was observed for L39Y and I56F.

To monitor the thermal stability of the new lactoglobulin variants, the ellipticity was measured as a function of temperature at 200 nm, which produced a very good signal to noise ratio. Considering the dependence of the denaturation profile on protein concentration, scanning speed, and pH, the measurements were conducted under identical conditions for all mutants. The constant protein concentration of 10–12 μM (corresponding to 0.2 mg/ml), much lower than previously applied in the thermal denaturation studies of BLG (de Wit, 2009), was used during the experiment. Due to the multi-stage denaturation process, the results of CD measurements cannot be analyzed numerically using the two-state model; therefore, the data are presented as the first derivative of ellipticity versus temperature (Fig. 4). Depending on the mutant, one or two transitions were observed, allowing the determination of the T_m of the most significant transitions (Table 3).

Generally, lactoglobulin variants containing mutations in the upper part of the binding pocket have higher thermal stability, and the increase of their T_m we observed was about 5 °C. Substitution I56F destabilizes the protein and decreases its T_m by 6.5 °C. The substitution of V92 by phenylalanine does not significantly affect the T_m, contrary to substitution by tyrosine which strongly destabilizes the protein. The additional peak, indicating an intermediate denaturation step, was observed in the range 40–60 °C for variants L39Y and F105L. Interestingly, these are the two mutants that deviate significantly in migration through the chromatography column.

To verify whether the main transition coincides with denaturation to a similar extent for each variant, the CD spectra at 95 °C were measured for samples previously subjected to thermal unfolding (Fig. 4). The high similarity of all CD spectra indicates the same conformation of lactoglobulin corresponding to the state of the molten globule (Qi et al., 1997, 1995).

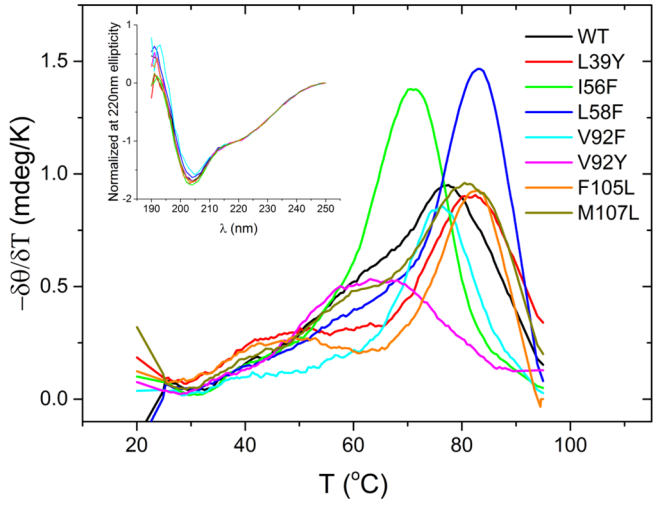

Fig. 4. Thermal denaturation profiles (ellipticity at 200 nm) represented as the first derivative of ellipticity. Inset: The CD spectra in far UV for 10 μM proteins after thermal denaturation in 50 mM phosphate buffer at 95 °C normalized at 220 nm.

3.5. pH-Induced protein transitions

To determine how the substitutions affect protein conformation at different pHs, the CD signal in the far-UV range and tryptophan fluorescence were analyzed in the pH range from 4 to 10. In order to normalize the fluorescence signal quality and to eliminate errors related to protein concentration, the results are presented as a ratio of intensity at 328 and 345 nm (Fig. S3). Lactoglobulin contains two tryptophan residues. The first, W19, is located in the β-barrel in a hydrophobic environment close to the bottom of the binding pocket, while the second, W61, is on the protein surface. The fluorescence study of the W19A variant (Katakura et al., 1994) indicated that W19 is responsible for 80% of the total fluorescence signal; hence λ_{max} was about 329 nm. Therefore, the measured ratio is proportional to the change in tryptophan exposure to the solvent, and its fluorescence quenching results from rearrangement of the tertiary structure of the tryptophan microenvironments.

Initially, the change of pH from 4 to 5 caused a significant increase in the 328 nm/345 nm fluorescence ratio. A further increase in pH resulted in a gradual decrease in the ratio for all variants except V92Y, for which a more rapid drop at pH above 8.5 was observed. Earlier studies performed for BLG isoform A have shown that in the same range

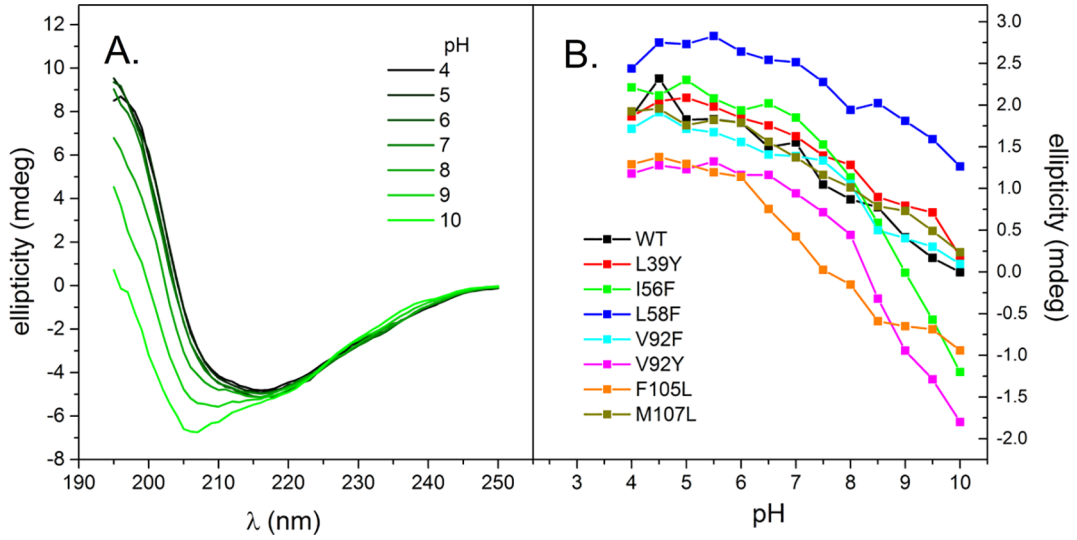

Fig. 5. The pH-induced changes of far-UV circular dichroism spectra. **(A)** An example of CD spectra at different pH recorded for I56F mutant in BAP buffers and 25 °C (spectra for other variants were similar). **(B)** The ellipticity at 200 nm as a function of pH.

of pH, the fluorescence intensity initially decreased until reaching a minimum value between pH 6 and 7 and then increased again at pH 9 (Renard et al., 1998).

The CD spectra obtained for different mutants were very similar in the pH range from 4 to 7 and showed no significant changes, but a decrease in the ellipticity of the 200 nm band was observed above pH 7 (Fig. 5A). This observation is consistent with previously published data (Taulier and Chalikian, 2001) and results from the increase of the fraction of unfolded polypeptide associated with base-induced denaturation. Therefore, the comparison of variants was made by monitoring the changes of ellipticity at 200 nm (Fig. 5B). To quantify changes, the secondary structure content was calculated on the basis of CD spectra. The α-helix and turn fractions do not change significantly and fluctuate around 13% and 22%, respectively, while an increase of pH is accompanied by an expansion of unfolded fraction from about 25% to above 30% at pH 10 and the proportional decrease of β-sheet content. The largest fraction of unfolded state was observed for V92Y and I56F, the least thermally stable proteins, while the smallest decrease in β-sheet content was observed for L58F, the mutant with the highest T_m, for which at pH greater than 9 no significant change of the unfolded fraction was observed. It suggests that the thermal and pH-induced transition may have a similar structural origin.

3.6. Palmitic acid binding

A palmitic acid (PLM) competitive binding assay was used to verify the influence of mutations on the protein's ability to bind this ligand inside the β-barrel. Because no optical response to PLM is observed in fluorescence studies, competition between ANS and PLM was used to monitor PLM binding (Collini et al., 2003, 2000). Before titration experiments, mutants and ANS were mixed in the same concentrations and molar ratio. In the presence of lactoglobulin, the fluorescence is emitted mainly by the protein-bound ANS and the formation of BLG-ANS complex increases the effective quantum efficiency of ANS fluorescence about 266 times (D'Alfonso et al., 1999). Therefore, assuming a similar quantum efficiency of fluorescence emitted by ANS bound to each variant, one can expect a similar fraction of ANS bound to each mutant.

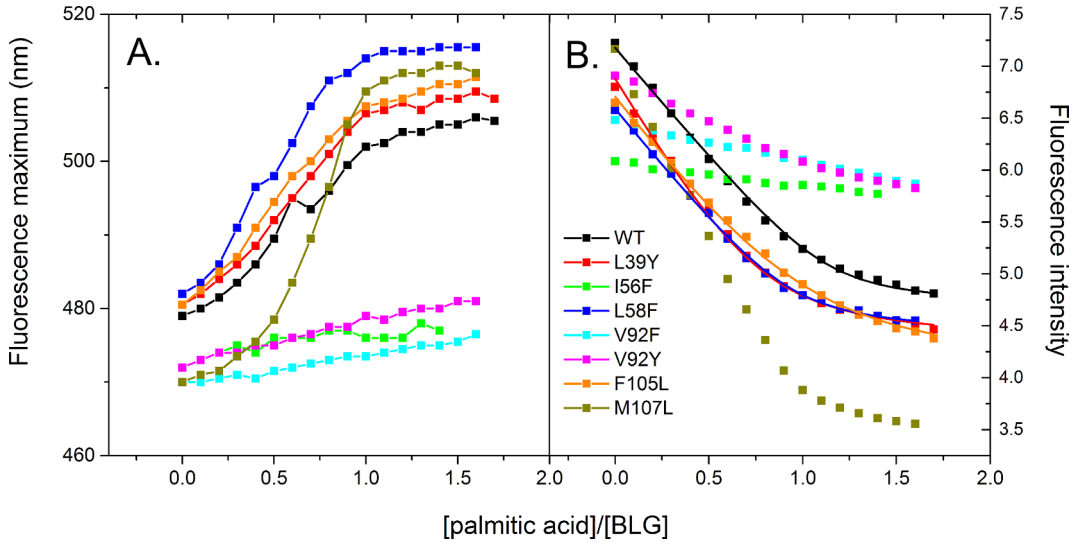

Fig. 6. The palmitic acid competitive binding assay. The changes of fluorescence maxima of ANS (**A**) and the changes of ANS fluorescence intensity (**B**) associated with PLM titration. Experiments performed for 5 μM BLG variants, 6 μM ANS in Tris-HCl pH 8.0 at 25 °C. The solid lines in panel B represent the best fits obtained with the dissociation model for variants: WT, L39Y, L58F, F105L.

Table 4
Parameters of palmitic acid binding determined in ANS competition experiments.

	n_{app}	K_{app} [μM]
WT	1.14 ± 0.03	0.16 ± 0.06
L39Y	0.81 ± 0.03	0.35 ± 0.09
L58F	0.95 ± 0.02	0.21 ± 0.04
F105L	1.05 ± 0.05	0.70 ± 0.30

However, it was observed that the initial values of ANS fluorescence are different for individual mutants and there are also differences in the shift of fluorescence maxima during titration (Fig. 6A). The above observation allowed us to divide studied variants into two groups: (1) with an initial maximum of fluorescence at about 470 nm (I56F, V92F, V92Y, M107L) and (2) with an initial maximum at about 480 nm (WT, L39Y, L58F, F105L). Because there is no crystal structure of BLG-ANS complex available to date, it is not possible to precisely define the ANS binding sites in BLG; however, the observation above may suggest a different position of ANS in the β-barrel of mutants from group (1) and (2). Our structural data indicate that these different ANS binding modes might be related to the depth of the binding pocket.

The decrease of ANS fluorescence intensity and the bathochromic shift of the fluorescence maximum was observed during PLM titration for WT, L39Y, L58F, F105L, and M107L mutants (Fig. 6A). Such changes can be interpreted as a reduction of the protein-bound ANS fraction due to ANS release from the BLG upon PLM binding. In variants with substitutions L39Y, L58F, F105L and M107L, the ability to bind PLM was retained, as indicated by the shape of titration curves (Fig. 6A). For I56F, V92F and V92Y, the fluorescence intensity only slightly decreased during titration with PLM. This observation can be explained in two possible ways: (1) PLM binding does not significantly affect protein-bound ANS or (2) the affinity of PLM to these variants is

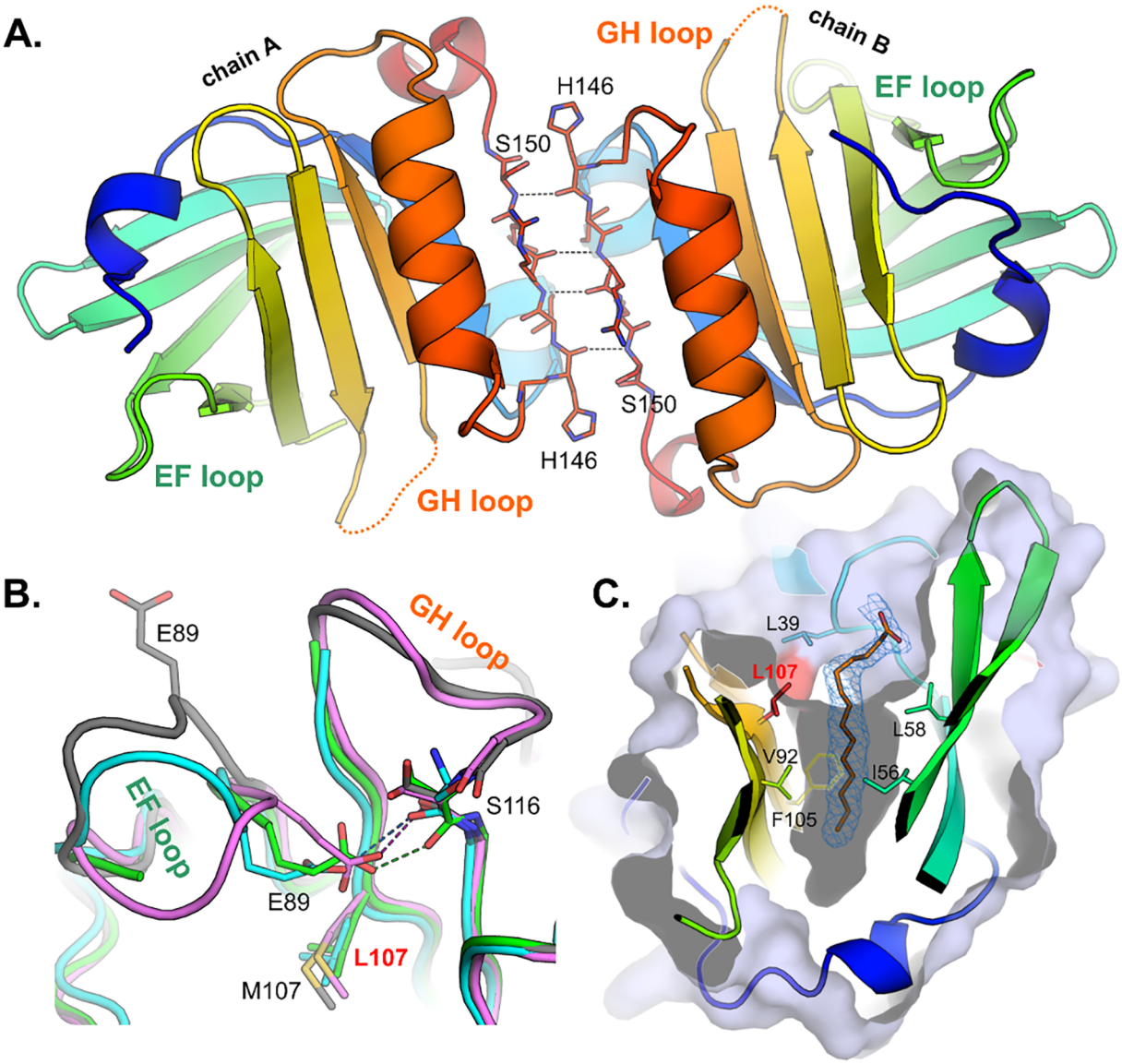

Fig. 7. (**A**) Dimer of M107L colored by rainbow scheme the same as applied in Fig. 1. The dimer is stabilized by hydrogen bonds (red dashed lines) between symmetry-related β-strands (residues 146–150). The disordered fragments of flexible GH loops are marked by dotted lines. (**B**) Conformation of EF loop in the chain A (green) and chain B (cyan) in the structure of M107L variant. Both chains were superimposed (Cα) to the lactoglobulin structure, and show an open (grey, PDB ID: 2BLG) and closed (pink, PDB ID: 3BLG) conformation of EF loop. Dashed lines represents hydrogen bonds between OE2 atom of E89 and carbonyl oxygen of S116. (**C**) The structure of variant M107L co-crystallized with myristic acid. Fatty acid has extended conformation. The electron density map (2FoFc) around ligand is shown at level 1.00 σ.

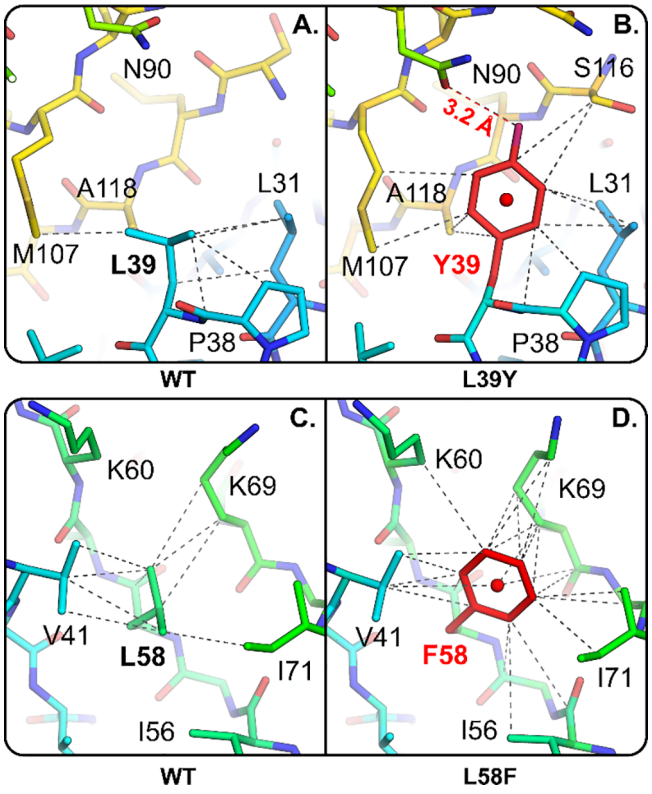

Fig. 8. Increased number of interactions at mutation sites in mutants L39Y and L58F in comparison to those present in WT protein (red dashes: hydrogen bond, grey dashes: C-H···π interactions or hydrophobic contacts in distance 3.3–4.5 Å; red sphere represents aromatic ring centroid). (**A**) Interactions of L39 in WT protein and interactions of (**B**) Y39 in L39Y variant. (**C**) The environment of L58 in WT protein and (**D**) environment of F58 in mutant L58F.

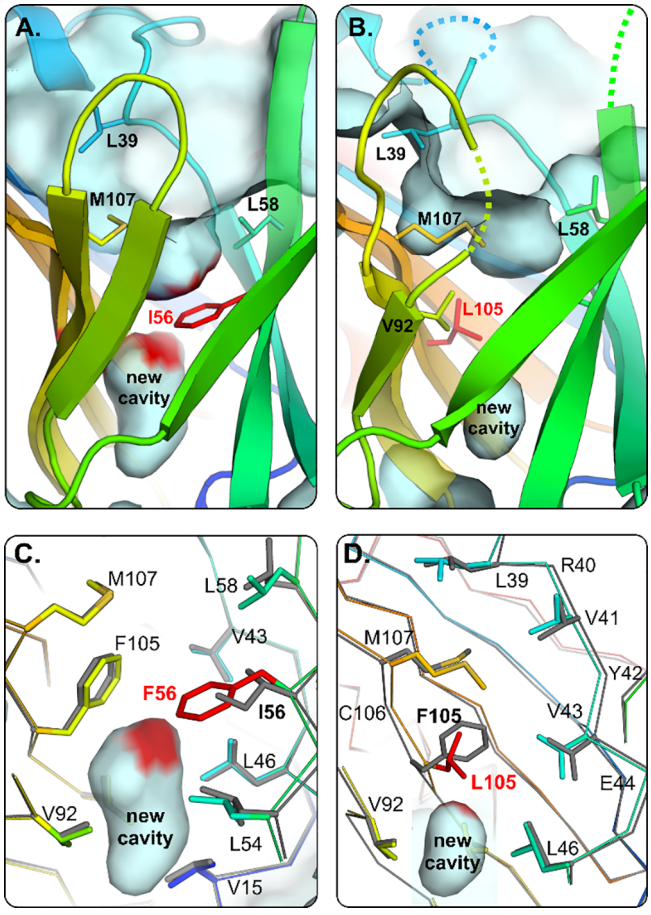

Fig. 9. Shortening of the binding pocket in mutant I56F (**A**) and F105L (**B**). Mutations I56F and F105L block access to the most hydrophobic part of the β-barrel and create new cavities at the barrel bottom. Solvent accessible surface was drawn using probe radius 1.4 Å, mutated residues are shown in red, dotted lines in figure (B) represents missing (disordered) loops in the structure F105L. (**C**) Side chains surrounding the new cavity in mutant I56F and positions of their counterparts in WT protein (grey). (**D**) Systematic shifts of residues 39–44 and 104–107 in the structure of F105L variant in comparison to their positions in WT protein (grey, PDB ID: 5HTE).

significantly lower compared to other variants. The fact that the initial fluorescence of these mutants was similar to other variants that could bind PLM, suggests that the latter explanation is more likely.

The quantitative analysis of PLM/mutant interaction was performed according to a simple dissociation model. Although this model is not general and fully applicable to describe the ANS/PLM competition, it allows the comparison of the BLG variants, as all measurements were done for the proteins with almost identical structures. Calculations were made only for the WT, L39Y, L58F and F105L variants showing similar initial values of bound ANS fluorescence and titration behavior. The calculated apparent values of dissociation constant and stoichiometry are presented in Table 4. The stoichiometry was about 1.0 PLM molecule per protein monomer. The only exception was L39Y variant for which n_{app} was close to 0.8, which could have been the result of partial protein denaturation and/or partial blocking of the binding pocket. The similarity of K_{app} indicates that L39Y, L58F, and F105L variants bind PLM with an affinity of the same order of magnitude as WT.

3.7. Crystal structure of lactoglobulin mutants

Crystals suitable for X-ray diffraction measurements were obtained for all mutants except for V92F and V92Y. The crystallographic studies (Table 1), revealed that most of the structures were in the $P3_221$ space group with the asymmetric unit (AU) containing a single protein chain, while a second dimer subunit was related by a crystallographic 2-fold axis. The only exceptions were structures of unliganded F105L ($C222_1$ crystal symmetry, single chain in AU) and M107L ($P22_12_1$ crystal symmetry, dimer in AU). As previously found for BLG (Loch et al., 2011), and confirmed later for its variants (Loch et al., 2018, 2016), the protein dimer is stabilized by four hydrogen bonds between H146, R148, S150, and their symmetrical counterparts (Fig. 7A). The crystallographic analysis showed that in the crystallization conditions, the mutations do not affect the structure of the dimer interface. The superposition of WT and variant dimers showed atomic shifts up to 0.85 Å for Cα atoms in both subunits. The observed changes seem to be the result of small differences in the unit cell parameters and the crystal packing rather than the effect of the mutation.

The crystal structures revealed that the β-barrel interior is flexible enough to accept some amino acid substitutions. The mutations were incorporated in the middle and the upper part of the binding pocket (Fig. 1, Fig. S1). Only small atom shifts have been observed for residues in the vicinity of the mutation site. Superposition of WT protein and mutants gave RMSD values in the range 0.2–0.3 Å for Cα atoms. Almost no changes were observed in the rigid protein core near W19, confirming that the differences detected in near-UV CD spectra (Fig. 3) are the result of discrepancies in protein dynamics in solution rather than permanent structural changes around W19. Because the pH of the crystallization solution was always higher than 7.0, it was expected that the EF loop in all structures would have an open conformation. Indeed, the crystal structures contained open conformations, indicating that the mutations did not affect the Tanford transition (Qin et al., 1998). The only exception was the structure of unliganded M107L variant, in

which the EF loop adopts an unusual, partially closed conformation (Fig. 7B).

Despite several crystallization experiments in conditions used for other mutants, we were not able to crystallize variants V92F and V92Y. These mutations are present in the middle part of the binding pocket, close to I56 and F105. As the aromatic substitution was in most cases well tolerated by the protein and did not influence crystallization, the origin of crystallization failure for both V92 variants remains unclear.

3.7.1. L39Y-(PLM)

Residue 39 is located at the β-barrel entrance. The side chain of the Y39 substitution fits into the cleft between the AB and GH loop and fills it almost completely (Fig. 8). The position of the tyrosine side chain is stabilized by a hydrogen bond between the hydroxyl group and N90 located on the EF loop (Fig. 8B). Although L39Y was crystallized without the addition of any ligand, Fourier difference maps revealed a strong, elongated positive density in the binding pocket (Fig. S4). The endogenous ligand was observed in all of the studied crystals of L39Y mutant obtained from two different purification runs. The size of the electron density corresponds well to the 16-carbon palmitic acid that has been modeled inside the binding pocket. The presence of endogenous ligand was previously observed in recombinant lactoglobulin, but it was not observed for protein purified using the modified purification protocol used herein (Loch et al., 2018, 2016). Fatty acids were not observed in any other lactoglobulin variants purified using this method. A comparison of the structure of L39Y and bovine β-lactoglobulin complex with palmitic acid (PDB ID: 3UEW), showed no significant differences in ligand position and conformation. Furthermore, the binding pocket geometry in the vicinity of the ligand is well preserved. The endogenous ligand does not directly interact with Y39.

3.7.2. I56F

Mutation I56F is located in the middle of the binding pocket, opposite M107. The aromatic ring of F56 partially fills the β-barrel interior, which makes the binding pocket shorter and creates a cavity at the bottom of the original binding pocket (Fig. 9A,C). Crystallization trials of I56F in presence of MYR failed, whereas the use of shorter 12-carbons long lauric acid for co-crystallization facilitated crystal growth. Although this variant was crystallized in the presence of lauric acid, the determined structure did not contain this fatty acid bound in the binding pocket or on the protein surface.

3.7.3. L58F and L58F-MYR

L58 is one of the residues that creates the hydrophobic environment in the upper part of the binding pocket. The introduction of phenylalanine at this position does not affect the conformation of the main chain or the shape of the binding pocket but greatly stabilizes the upper part of binding site by extended the network of hydrophobic contacts (Fig. 8D). Mutant L58F was crystallized both in the presence and absence of myristic acid. The position of the substituted phenylalanine was essentially the same for the two structures. When compared to the WT protein, the co-crystallized structure shows that this substitution did not change either the mode of ligand binding or its conformation (Fig. S4).

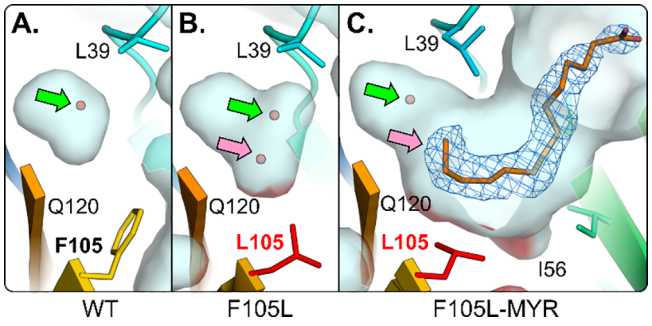

Fig. 10. Structural changes in mutant F105L. (**A**) A green arrow points to a water molecule trapped in the conserved cavity positioned between L39 and Q120 located in hydrophobic core in WT protein (PDB ID: 5HTE). (**B**) This cavity is enlarged in F105L mutant and an additional water molecule is present (pink arrow). (**C**) When myristic acid is bound to the F105L variant, the end of its chain (pink arrow) displaces the second water molecule from the enlarged cavity. The electron density map around the ligand is shown at 1.00 σ level. Solvent accessible surface was drawn with a 1.4 Å probe radius.

3.7.4. F105L and F105L-MYR

The F105L mutant was also crystallized in the presence and absence of myristic acid. The side chain of residue 105, is positioned slightly deeper in the β-barrel than M107 (Fig. 1). Crystals of the apo-form of F105L variant always diffracted X-rays poorly, suggesting the presence of internal disorder. The crystal structure of F105L revealed strong conformational disorder of the C- and N-terminal fragments and all flexible loops. The protein core, including L105, was easily visible in the electron density map. The crystal structure of the unliganded F105L variant showed a systematic shift by about 0.5 Å of residues 104–107 located on β-strand G towards residues 39–44 on β-strand B. This displacement resulted in enlarging of internal cavity located in the hydrophobic core (in the vicinity of residues L39 and Q120, Fig. 10) and in shortening of the binding pocket (Figs. 9 and 10). Despite that, the protein retained the ability to bind myristic acid. The structure of the F105L-MYR complex showed that the fatty acid in the binding pocket adopts a bent conformation, unusual for fatty acids bound to BLG (Fig. S5). The end of the hydrocarbon chain is located in the space which in unliganded protein, and other structures presented herein, is usually occupied by the M107 side chain (Fig. S5). Accommodation of the ligand in this position required not only displacement of the M107 side chain and water from the extended cavity but also some movement of EF-loop and β-strands F and G, demonstrating the ability of the binding site to adapt to the presence of fatty acid (Fig. 10). The combination of the movement of M107 and reducing the size of the side chain at position 105, creates a binding pocket that can accommodate a number of other molecules and has even exposed main chain carbonyls for hydrogen bonding.

3.7.5. M107L and M107L-MYR

The unliganded M107L variant crystallized with two copies in the asymmetric unit, with an unusual conformation of the EF loop in subunit B. In that subunit, E89, a residue involved in the Tanford transition, occupies a position similar to the one observed in structures with EF loop in closed conformation (Loch et al., 2015b, 2014), while the rest of the loop adopts an open conformation (Fig. 7B). Such a conformation has not been observed in other structures of β-lactoglobulin to date (Loch et al., 2014, 2015b, 2019; Qin et al., 1998). In subunit A, residues 90–95 are disordered, but the position of other residues, in particular E89, is similar to those observed in subunit B.

In the structure of the M107L variant co-crystallized with myristic acid, the EF loop is in the typical open conformation. The substitution of M107 by leucine widens the entrance to the binding pocket in the region of AB loop and induces the slight shifts of E55-I56 and I71-K69 atoms, making the binding pocket more narrow in the middle. However, these changes are reversible and do not prevent the binding of myristic acid. Rotation of the L107 side chain opens access to the lower part of the binding pocket and allows a myristic acid molecule to bind in the same position and extended conformation as previously observed in structures of other lactoglobulin-fatty acid complexes (Fig. 7C and Fig. S4) (Loch et al., 2013a, 2012).

Table 5
Overall characteristics of library of new lactoglobulin mutants created by structure-based design approach (n.a. = not applicable).

Mutation	L39Y	I56F	L58F	V92F	V92Y	F105L	M107L
dimerization constant changes	no changes	no changes	no changes	no changes	no changes	no changes	no changes
secondary structure changes	no changes	no changes	no changes	no changes	no changes	no changes	no changes
thermal stability	increased	decreased	increased	no changes	decreased	increased	increased
chemical stability	increased	increased	increased	increased	decreased	increased	no changes
pH-dependent behavior	no changes	small changes	no changes	no changes	small changes	no changes	no changes
binding of palmitic acid	no change in affinity	no affinity	no change in affinity	no affinity	no affinity	no change in affinity	change in affinity[2]
crystallizability[1]	yes	yes	yes	no	no	yes	yes
endogenous ligand	yes	no	no	n.a.	n.a.	no	no
binding pocket	no changes	shorter	no changes	n.a.	n.a.	shorter and wider	no changes
fatty acid conformation	extended	n.a.	extended	n.a.	n.a.	bent	extended

[1]at conditions similar to crystallization of WT lactoglobulin.
[2]lower intensity of fluorescence maximum suggests changes in binding affinity of ANS and/or palmitic acid.

4. Discussion

4.1. Overall protein structure, dimerization constant and pH-dependent behavior

Bovine β-lactoglobulin is a model lipocalin, broadly used in many biochemical, biophysical, and nutrition-related studies. Lactoglobulin mutagenesis has been previously investigated by different research groups, but only for residues located outside the binding pocket (supplement Table S4). Furthermore, no studies on soluble recombinant β-lactoglobulin expressed in *E. coli* have been reported, except for work by Cho et al. (Cho et al., 1994) who produced incorrectly folded protein in *E.coli* inclusion bodies that were subsequently re-folded. In our work, seven soluble and correctly folded lactoglobulin mutants with single-site mutations inside the binding pocket (L39Y, I56F, L58F, V92F, V92Y, F105L and M107L) have been successfully produced in bacteria, purified, and examined. The impact of substitutions on the protein secondary and tertiary structure, as examined by CD and X-ray crystallography, is negligible (Table 5). Similar conclusions can be drawn from the analysis of tryptophan fluorescence spectra. In general, the mutations do not affect the pH-dependent behavior of BLG; however, some small discrepancies (Fig. 5) were observed for V92Y and I56F, the least thermally stable proteins. A summary of the most important properties of lactoglobulin mutants is presented in Table 5.

The size-exclusion chromatography, followed by the structural analysis, confirmed that the mutations did not affect the quaternary structure of any of the variants in solution and in the crystalline phase. The dimerization constants determined using ITC are similar for all variants (Tables 2, and 5); however, the different contributions of ΔH_{dim} and $T\Delta S_{dim}$ indicate that mutations indirectly affect the mechanism of dimer formation. The similar values of ΔG_{dim} observed for all mutants are probably the results of the enthalpy–entropy compensation. The mutagenesis was carried out in a region distant from the dimer interface, and the observed discrepancies of the above parameters should not be attributed to altered dynamics, conformation, or protonation state of ionizable groups, but might originate from differences in the hydration of dimer interface. Osmotic stress measurements and observation of the dimer in the crystal structure prove that a large number of water molecules are incorporated into the dimer interface upon subunit association (Bello et al., 2008). The estimated upper limits of the entropy and enthalpy of transferring a water molecule from bulk solvent to the interface are −30 J/mol/K and −16 kJ/mol at 298 K, respectively (Ladbury, 1996). In consequence, even a small change of hydration could explain the observed changes in thermodynamic parameters. The only exception is mutant L39Y, with the ratio of ΔH_{dim} to ΔS_{dim} deviating from the other variants (Fig. 2A). This suggests that a different, unidentified mechanism may influence dimerization of L39Y. It was shown earlier for palmitic acid (Wang et al., 1998) and SDS (Gutiérrez-Magdaleno et al., 2013) that an aliphatic ligand bound to BLG could trigger dimerization, so it may be the factor responsible for abnormal migration of L39Y during size-exclusion chromatography.

4.2. Chemical and thermal stability

Investigations of chemical and thermal stability of the new lactoglobulin variants revealed that each single mutation affects the protein in a different way (Tables 3 and 5). The largest increase of thermal stability was observed for variants L39Y and L58F, smaller for M107L and F105L. For L39Y, the existence of ligand bound fraction can affect thermal and chemical stability. It has been previously demonstrated by differential scanning calorimetry that BLG bound to palmitic acid is more resistant to thermal denaturation than unliganded protein. The presence of palmitic acid shifted the T_m from 70.5 to 78 °C (Puyol et al., 1994). It was also reported that bound aliphatic ligand (SDS or palmitate) increased lactoglobulin resistance to urea-induced unfolding (Creamer, 1995).

Interestingly, the thermal-stabilizing effect of the F105L mutation was also observed in variants possessing additional substitutions: F105L/L39A and F105L/L39A/M107F (Loch et al., 2018) while substitution I56F decreased thermal stability both alone and in the presence of other substitutions: I56F/L39A or I56F/L39A/M107F (Loch et al., 2018). These findings indicate that some properties of single mutants are preserved in the presence of additional mutations.

Results of previous studies indicate that at a concentration below 25 mg/ml the thermal denaturation of BLG is a multi-stage process (Qi et al., 1997). The temperature of dimer dissociation was predicted to be lower than 55 °C (de Wit, 2009), so in the higher temperature BLG should exist as a monomer. At the temperature above 80 °C the breakage and exchange of disulfide bridges occurs, leading to the protein aggregation (de la Fuente et al., 2002) and partial irreversible denaturation (Qi et al., 1995). Total, irreversible lactoglobulin unfolding appears at about 130 °C (Petit et al., 2011). Because the samples were heated to only 95 °C during thermal denaturation in our measurements, it can be assumed that the variants were partially irreversibly denatured.

The dissociation of the BLG dimer leads to a consecutive transition visible as the shoulder or small peak on the low-temperature side of thermograms recorded at low protein concentration. Such a transition should be visible for all mutants in CD signal; however, the peak in the 40–60 °C region was only clearly distinguishable for L39Y and F105L. The same effect, visible as a shoulder on the melting curve, was observed for other variants possessing F105L mutation (Loch et al., 2018). The determined differences in T_m values refer mainly to the effect of a single mutation on monomer stability. The lack of correlation between the thermal and chemical stability of BLG results from the complexity of these processes. The incomplete reversibility is observed not only for thermal denaturation but also for urea-induced denaturation (Yagi et al., 2003). Therefore, for each variant, measurements were performed at identical conditions (protein concentration, pH, ionic strength, heating rate). The high similarity of the native and denatured

states was also confirmed by CD spectra. Additionally, BLG did not precipitate on heating in the temperature range used, which makes the results reliable. Hence, ΔG^0 and T_m are apparent parameters that quantitatively describe the changes in protein stability caused by mutations. In general, the substitutions introduced increased the chemical and thermal stability of the variants. The two exceptions are V92Y, which decrease both stabilities, and I56F, which decreased the thermal stability but increased the chemical stability.

4.3. Ligand binding and crystal structures

Our previous studies showed that the binding mode of myristic and palmitic acid is almost identical (Loch et al., 2012). Therefore, the crystal structures of LGB variants and their complexes with MYR can be used to interpret results of ANS/PLM competitive studies. The crystal structures revealed that mutations either do not significantly influence the binding pocket geometry (L39Y and L58F) or reduce the depth of the binding site (Fig. 9). The crystal structures revealed that local rearrangements in the β-barrel interior might also affect the conformation of the fatty acid. In mutants L39Y, L58F, and M107L, the ligand is bound in extended conformation (Figs. S4 and 7C), while in the F105L variant, the shortened binding pocket is wide enough to accept an aliphatic chain in a bent conformation, which is not typical for fatty acids bound to BLG (Figs. 9, 10). Structural studies of the I56F mutant revealed that its binding pocket is too short and the aromatic ring of F56 makes accommodating a 14-carbon MYR impossible. Because the binding of endogenous ligands prior to and during purification can present a barrier to desirable molecule binding, mutations that shorten the binding pocket are advantageous.

The observed structural changes provide an explanation of results from fluorescence ligand binding studies. The fluorescence intensity changes, the shift of its maximum, and values of calculated K_{app} (Table 4) indicate that variants L39Y, L58F, and F105L retained the PLM binding mode similar to that of WT-lactoglobulin. Their ability to bind fatty acid molecules in the β-barrel was confirmed by the crystal structures. For variant M107L, the initial values of fluorescence intensity and maximum position at 470 nm correspond to those observed for mutants I56F and V92F/Y. During titration, the M107L fluorescence maximum was shifted close to that observed for L39Y, L58F, and F105L but with lower intensity (Fig. 6). This may be related to the presence of small conformational changes accompanying fatty acid binding in the pocket as observed in the crystal structure.

Analysis of the binding pocket geometry in I56F reveals changes that might significantly reduce its affinity to PLM. This observation explains why the intensity of ANS fluorescence for this variant only slightly decreased during titration with PLM. Since the V92F and V92Y mutants showed very similar titration behavior, it can be assumed that the binding pocket geometry is permanently distorted in these variants in a way similar to that observed in I56F.

The lower stoichiometry of binding (about 0.80) observed in solution for L39Y can be explained by the presence of endogenous ligand (Fig. 8A). The hydrogen bond between the Y39 hydroxyl group and N90 amide oxygen (Fig. 8B), which is not present in WT protein or other variants, may affect conformational changes of EF and GH loops and facilitate retention of endogenous ligand in the β-barrel. It is also possible that both liganded and unliganded forms of L39Y co-exist in solution, but the crystallization process selects only molecules with bound fatty acid. Such selectivity was previously observed for goat and sheep β-lactoglobulin (Loch et al., 2019, 2015b).

4.4. Most promising candidates for further studies

The effects of amino acid substitutions were observed mainly at the local level, e.g., rearrangement of binding pocket geometry. However, mutations also influenced the global properties of the protein as chemical and thermal stability but not the dimerization constant or pH-dependent conformational behavior. Each mutation affects properties of lactoglobulin in an individual way, even though the mutations were introduced in the same region of the molecule. Based on the results of biophysical and structural studies, we propose the L39Y, I56F, L58F, and F105L mutations as the most promising BLG modifications for future advanced mutagenesis (Table 5). The mutation of F105 essentially opens up a cavity that is large enough to bind other molecules. A sequestered water molecule is in this location in some structures. Furthermore, there are several nearby atoms that can form hydrogen bonds. This makes this mutation an attractive substitution when designing new variants for potential therapeutic agents.

Mutations L58F and L39Y increase chemical and thermal stability and can be introduced to BLG when protein with higher urea- and/or temperature-resistance is required. Such a protein might be advantageous for use in food-related or nutritional studies when high-temperature stability is a priority. Mutants with shortened binding pockets, like I56F and F105L, are excellent starting points for designing lactoglobulin variants with affinity to selected drugs. Minor disadvantages, such as slightly decreased thermal stability (I56F) and increased structural flexibility (F105L) demonstrated during abnormal migration through the size-exclusion column, do not outweigh their advantages: reduced affinity to fatty acids (I56F) or re-shaped and broadened binding pocket (F105L). New variants based on I56F and F105L, containing additional mutations: I56F/L39A, I56F/L39A/M107F, F105L/L39A and F105L/L39A/M107F were already produced and characterized (Loch et al., 2018). Studies of their complexes revealed, among other original biochemical features, the stereoselective binding of chlorpromazine chiral conformers (Loch et al., 2018).

5. Summary

This article used a simple and non-expensive approach for the design of lactoglobulin variants with the goal of expanding the range of molecules that can be bound. Lactoglobulin nanobodies have already shown (Bijari et al., 2019) great promise as a drug delivery system capable of targeting specific cell types. Immobilized lactoglobulin can also be used for blood detoxification in extracorporeal dialysis systems (Tumlin, 2019). Both of these therapeutic approaches require molecules that can efficiently bind a range of small molecules, and the benefits of using BLG in these processes warrant exploring non-natural lactoglobulin variants that can be easily expressed. The mutations we made were based on an analysis of the occurrence of residues in structural homologs possessing distant sequence identity. Seven lactoglobulin variants with mutation inside binding pocket were correctly folded and stable. The thorough characterization by fluorescence, circular dichroism, isothermal titration calorimetry, size-exclusion chromatography and X-ray structural investigations revealed both local and global effects of substitutions and showed that each variant possesses a unique combination of individual properties that can be used for further modifications.

Taking a stepwise approach and looking at the effects of the individual mutations, as has been presented here, can lead to a strategy for the development of more complex variants. An in-depth understanding of the effects of each individual substitution can be extremely useful in developing better bio-therapeutics or enzymes with more desirable kinetics or substrates. The L39Y, I56F, L58F, and F105L mutations show the most promise for incorporations into more complex mutants that could be therapeutically effective. The work described herein shows that the binding pocket of lactoglobulin can accept mutations while simultaneously increasing its stability, thereby increasing the likelihood of the use of lactoglobulin in advanced therapeutics.

6. Grants

Studies were supported by the Polish National Science Centre (Poland). Grant Number: 2012/05/B/ST5/00278.

Declaration of Competing Interest

The authors declare that they have no known competing financial interests or personal relationships that could have appeared to influence the work reported in this paper.

Acknowledgments

Authors would like to acknowledge the participation of Kinga Kaczor, Monika Siuda and Mateusz Gotkowski in protein expression, purification and crystallization.

Author Contributions

P. Bonarek: performed ITC, fluorescence, SEC, CD, preparation of manuscript draft**. J. I. Loch**: performed protein expression, purification, crystallization, X-ray data collection, structure solution and refinement, data analysis, PDB deposition, preparation of manuscript draft. **M. Tworzydło**: site-directed mutagenesis. **D. R. Cooper**: participation in interpretation of structural data, language editing and proofreading the text. **K. Milto:** participation in ITC, fluorescence, SEC and CD measurements**, P. Wróbel:** participation in structural analysis and preparation of revised manuscript version, **K. Kurpiewska:** participation in protein crystallization and X-ray data collection, **K. Lewinski:** supervision of the project, participation in data analysis, manuscript writing and preparation of the final manuscript.

Appendix A. Supplementary data

Supplementary data to this article can be found online at https://doi.org/10.1016/j.jsb.2020.107493.

References

Anderson, G.P., Hohlbaum, A., Jensen, K., Bähre, A., Gille, H., 2015. Discovery of PRS-060, an inhalable CD123/IL4Ra/TH2 blocking anti-asthmatic anticalin protein re-engineered from endogenous lipocalin-1. Eur. Respir. J 46.

Barkovskiy, M., Ilyukhina, E., Dauner, M., Eichinger, A., Skerra, A., 2019. An engineered lipocalin that tightly complexes the plant poison colchicine for use as antidote and in bioanalytical applications. Biol. Chem. 400, 351–366. https://doi.org/10.1515/hsz-2018-0342.

Bello, M., Pérez-Hernández, G., Fernández-Velasco, D.A., Arreguín-Espinosa, R., García-Hernández, E., 2008. Energetics of protein homodimerization: Effects of water sequestering on the formation of β-lactoglobulin dimer. Proteins Struct. Funct. Bioinforma. 70, 1475–1487. https://doi.org/10.1002/prot.21639.

Bello, M., Portillo-Téllez, M., del, C., García-Hernández, E., 2011. Energetics of ligand recognition and self-association of bovine β-lactoglobulin: differences between variants A and B. Biochemistry 50, 151–161. https://doi.org/10.1021/bi1016155.

Bijari, N., Ghobadi, S., Derakhshandeh, K., 2019. β-lactoglobulin-irinotecan inclusion complex as a new targeted nanocarrier for colorectal cancer cells. Res. Pharm. Sci. 14, 216–227. https://doi.org/10.4103/1735-5362.258488.

Britton, H.T.S., Robinson, R.A., 1931. CXCVIII.—Universal buffer solutions and the dissociation constant of veronal. J. Chem. Soc. 1456–1462. https://doi.org/10.1039/JR9310001456.

Cho, Y., Gu, W., Watkins, S., Lee, S.P., Kim, T.R., Brady, J.W., Batt, C.A., 1994. Thermostable variants of bovine beta-lactoglobulin. Protein Eng. 7, 263–270.

Collini, M., D'Alfonso, L., Baldini, G., 2000. New insight on beta-lactoglobulin binding sites by 1-anilinonaphthalene-8-sulfonate fluorescence decay. Protein Sci. https://doi.org/10.1110/ps.9.10.1968.

Collini, M., D'Alfonso, L., Molinari, H., Ragona, L., Catalano, M., Baldini, G., 2003. Competitive binding of fatty acids and the fluorescent probe 1–8-anilinonaphthalene sulfonate to bovine beta-lactoglobulin. Protein Sci. 12, 1596–1603. https://doi.org/10.1110/ps.0304403.

Creamer, L.K., 1995. Effect of sodium dodecyl sulfate and palmitic acid on the equilibrium unfolding of bovine beta-lactoglobulin. Biochemistry 34, 7170–7176.

Creamer, L.K., Parry, D.A., Malcolm, G.N., 1983. Secondary structure of bovine beta-lactoglobulin B. Arch. Biochem. Biophys. 227, 98–105. https://doi.org/10.1016/0003-9861(83)90351-x.

D'Alfonso, L., Collini, M., Baldini, G., 2002. Does β-Lactoglobulin Denaturation Occur via an Intermediate State? † Biochemistry 41, 326–333. https://doi.org/10.1021/bi0115028.

D'Alfonso, L., Collini, M., Baldini, G., 1999. Evidence of heterogeneous 1-anilino-naphthalene-8-sulfonate binding to β-lactoglobulin from fluorescence spectroscopy. Biochim. Biophys. Acta - Protein Struct. Mol. Enzymol. 1432, 194–202. https://doi.org/10.1016/S0167-4838(99)00105-3.

Dauner, M., Skerra, A., 2019. Scavenging Bacterial Siderophores with Engineered Lipocalin Proteins as an Alternative Antimicrobial Strategy. ChemBioChem cbic. 201900564. doi: 10.1002/cbic.201900564.

de la Fuente, M.A., Singh, H., Hemar, Y., 2002. Recent advances in the characterisation of heat-induced aggregates and intermediates of whey proteins. Trends Food Sci. Technol. 13, 262–274. https://doi.org/10.1016/S0924-2244(02)00133-4.

de Wit, J.N., 2009. Thermal behaviour of bovine β-lactoglobulin at temperatures up to 150°C. a review. Trends Food Sci. Technol. 20, 27–34. https://doi.org/10.1016/j.tifs.2008.09.012.

Eggenstein, E., Eichinger, A., Kim, H.-J., Skerra, A., 2014. Structure-guided engineering of Anticalins with improved binding behavior and biochemical characteristics for application in radio-immuno imaging and/or therapy. J. Struct. Biol. 185, 203–214. https://doi.org/10.1016/j.jsb.2013.03.009.

Evans, P.R., Murshudov, G.N., 2013. How good are my data and what is the resolution? Acta Crystallogr D. Biol. Crystallogr. 69, 1204–1214. https://doi.org/10.1107/S0907444913000061.

Frappier, V., Chartier, M., Najmanovich, R.J., 2015. ENCoM server: exploring protein conformational space and the effect of mutations on protein function and stability. Nucleic Acids Res. 43, W395–W400. https://doi.org/10.1093/nar/gkv343.

Gebauer, M., Skerra, A., 2012. Anticalins small engineered binding proteins based on the lipocalin scaffold. Methods Enzymol. 503, 157–188. https://doi.org/10.1016/B978-0-12-396962-0.00007-0.

Ghalandari, B., Divsalar, A., Saboury, A.A., Parivar, K., 2014. The new insight into oral drug delivery system based on metal drugs in colon cancer therapy through β-lactoglobulin/oxali-palladium nanocapsules. J. Photochem. Photobiol. B Biol. 140, 255–265. https://doi.org/10.1016/j.jphotobiol.2014.08.003.

Gille, H., Hülsmeyer, M., Trentmann, S., Matschiner, G., Christian, H.J., Meyer, T., Amirkhosravi, A., Audoly, L.P., Hohlbaum, A.M., Skerra, A., 2016. Functional characterization of a VEGF-A-targeting Anticalin, prototype of a novel therapeutic human protein class. Angiogenesis 19, 79–94. https://doi.org/10.1007/s10456-015-9490-5.

Gutiérrez-Magdaleno, G., Bello, M., Portillo-Téllez, M.C., Rodríguez-Romero, A., García-Hernández, E., 2013. Ligand binding and self-association cooperativity of β-lactoglobulin. J. Mol. Recognit. 26, 67–75. https://doi.org/10.1002/jmr.2249.

Hohlbaum, A.M., Gille, H., Trentmann, S., Kolodziejczyk, M., Rattenstetter, B., Laarakkers, C.M., Katzmann, G., Christian, H.J., Andersen, N., Allersdorfer, A., Olwill, S.A., Meibohm, B., Audoly, L.P., Swinkels, D.W., van Swelm, R.P.L., 2018. Sustained plasma hepcidin suppression and iron elevation by Anticalin-derived hepcidin antagonist in cynomolgus monkey. Br. J. Pharmacol. 175, 1054–1065. https://doi.org/10.1111/bph.14143.

Jayat, D., Gaudin, J.-C., Chobert, J.-M., Burova, T.V., Holt, C., McNae, I., Sawyer, L., Haertlé, T., 2004. A recombinant C121S mutant of bovine beta-lactoglobulin is more susceptible to peptic digestion and to denaturation by reducing agents and heating. Biochemistry 43, 6312–6321. https://doi.org/10.1021/bi0362469.

Jenkins, T.P., Fryer, T., Dehli, R.I., Jürgensen, J.A., Fuglsang-Madsen, A., Føns, S., Laustsen, A.H., 2019. Toxin neutralization using alternative binding proteins. Toxins (Basel). https://doi.org/10.3390/toxins11010053.

Kabsch, W., 2010. Integration, scaling, space-group assignment and post-refinement. Acta Crystallogr. D. Biol. Crystallogr. 66, 133–144. https://doi.org/10.1107/S0907444909047374.

Katakura, Y., Ametani, A., Totsuka, M., Nagafuchi, S., Kaminogawa, S., 1999. Accelerated secretion of mutant beta-lactoglobulin in Saccharomyces cerevisiae resulting from a single amino acid substitution. Biochim. Biophys. Acta 1432, 302–312.

Katakura, Y., Totsuka, M., Ametani, A., Kaminogawa, S., 1994. Tryptophan-19 of beta-lactoglobulin, the only residue completely conserved in the lipocalin superfamily, is not essential for binding retinol, but relevant to stabilizing bound retinol and maintaining its structure. Biochim. Biophys. Acta 1207, 58–67.

Kayani, Z., Bordbar, A.-K., Firuzi, O., 2018. Novel folic acid-conjugated doxorubicin loaded β-lactoglobulin nanoparticles induce apoptosis in breast cancer cells. Biomed. Pharmacother. 107, 945–956. https://doi.org/10.1016/J.BIOPHA.2018.08.047.

Kazem-Farzandi, N., Taheri-Kafrani, A., Haertlé, T., 2015. β-lactoglobulin mutation Ala86Gln improves its ligand binding and reduces its immunoreactivity. Int. J. Biol. Macromol. 81, 340–348. https://doi.org/10.1016/J.IJBIOMAC.2015.08.013.

Krug, R.R., Hunter, W.G., Grieger, R.A., 1976. Statistical interpretation of enthalpy-entropy compensation. Nature 261, 566–567. https://doi.org/10.1038/261566a0.

Kurpiewska, K., Biela, A., Loch, J.I., Lipowska, J., Siuda, M., Lewiński, K., 2019. Towards understanding the effect of high pressure on food protein allergenicity: β-lactoglobulin structural studies. Food Chem. 270, 315–321. https://doi.org/10.1016/J.FOODCHEM.2018.07.104.

Ladbury, J.E., 1996. Just add water! The effect of water on the specificity of protein-ligand binding sites and its potential application to drug design. Chem. Biol. 3, 973–980. https://doi.org/10.1016/S1074-5521(96)90164-7.

Lagassé, H.A.D., Alexaki, A., Simhadri, V.L., Katagiri, N.H., Jankowski, W., Sauna, Z.E., Kimchi-Sarfaty, C., 2017. Recent advances in (therapeutic protein) drug development. F1000Research 6, 113. doi: 10.12688/f1000research.9970.1.

Laptenok, S.P., Visser, N. V, Engel, R., Westphal, A.H., Van Hoek, A., Van Mierlo, C.P.M., Van Stokkum, I.H.M., Van Amerongen, H., Visser, A.J.W.G., 2011. A General Approach for Detecting Folding Intermediates from Steady-State and Time-Resolved Fluorescence of Single-Tryptophan-Containing Proteins. doi: 10.1021/bi101965d.

Leilabadi-Asl, A., Divsalar, A., Saboury, A.A., Parivar, K., 2018. Probing the interaction of two chemotherapeutic drugs of oxali-palladium and 5-fluorouracil simultaneously with milk carrier protein of β-lactoglobulin. J. Biol. Macromol. Int. https://doi.org/10.1016/j.ijbiomac.2018.01.067.

Liu, C., Liu, Z., Sun, X., Zhang, S., Wang, S., Feng, F., Wang, D., Xu, Y., 2018. Fabrication and characterization of β-lactoglobulin-Based Nanocomplexes Composed of Chitosan Oligosaccharides as Vehicles for Delivery of Astaxanthin. J. Agric. Food Chem. 66, 6717–6726. https://doi.org/10.1021/acs.jafc.8b00834.

Loch, J., Bonarek, P., Lewiński, K., 2019. Conformational flexibility and ligand binding properties of ovine β-lactoglobulin. Acta Biochim. Pol. https://doi.org/10.18388/abp.2019_2883.
Loch, J., Polit, A., Górecki, A., Bonarek, P., Kurpiewska, K., Dziedzicka-Wasylewska, M., Lewiński, K., 2011. Two modes of fatty acid binding to bovine β-lactoglobulin—crystallographic and spectroscopic studies. J. Mol. Recognit. 24, 341–349. https://doi.org/10.1002/jmr.1084.
Loch, J.I., Bonarek, P., Polit, A., Jabłoński, M., Czub, M., Ye, X., Lewiński, K., 2015a. β-Lactoglobulin interactions with local anaesthetic drugs – crystallographic and calorimetric studies. Int. J. Biol. Macromol. 80, 87–94. https://doi.org/10.1016/j.ijbiomac.2015.06.013.
Loch, J.I., Bonarek, P., Polit, A., Riès, D., Dziedzicka-Wasylewska, M., Lewiński, K., 2013a. Binding of 18-carbon unsaturated fatty acids to bovine β-lactoglobulin—Structural and thermodynamic studies. Int. J. Biol. Macromol. 57, 226–231. https://doi.org/10.1016/j.ijbiomac.2013.03.021.
Loch, J.I., Bonarek, P., Polit, A., Świątek, S., Czub, M., Ludwikowska, M., Lewiński, K., 2015b. Conformational variability of goat β-lactoglobulin: Crystallographic and thermodynamic studies. Int. J. Biol. Macromol. 72, 1283–1291. https://doi.org/10.1016/J.IJBIOMAC.2014.10.031.
Loch, J.I., Bonarek, P., Polit, A., Swiątek, Ś., Dziedzicka-Wasylewska, M., Lewiński, K., 2013b. The differences in binding 12-carbon aliphatic ligands by bovine β-lactoglobulin isoform A and B studied by isothermal titration calorimetry and X-ray crystallography. J. Mol. Recognit. 26, 357–367. https://doi.org/10.1002/jmr.2280.
Loch, J.I., Bonarek, P., Tworzydło, M., Łazińska, I., Szydłowska, J., Lipowska, J., Rzęsikowska, K., Lewiński, K., 2018. The engineered β-lactoglobulin with complementarity to the chlorpromazine chiral conformers. Int. J. Biol. Macromol. 114, 85–96. https://doi.org/10.1016/J.IJBIOMAC.2018.03.074.
Loch, J.I., Bonarek, P., Tworzydło, M., Polit, A., Hawro, B., Łach, A., Ludwin, E., Lewiński, K., 2016. Engineered β-Lactoglobulin Produced in E. coli: Purification. Biophys. Struct. Characteris. Mol. Biotechnol. 58, 605–618. https://doi.org/10.1007/s12033-016-9960-z.
Loch, J.I., Molenda, M., Kopeć, M., Swiątek, S., Lewiński, K., 2014. Structure of two crystal forms of sheep β-lactoglobulin with EF-loop in closed conformation. Biopolymers 101, 886–894. https://doi.org/10.1002/bip.22471.
Loch, J.I., Polit, A., Bonarek, P., Olszewska, D., Kurpiewska, K., Dziedzicka-Wasylewska, M., Lewiński, K., 2012. Structural and thermodynamic studies of binding saturated fatty acids to bovine β-lactoglobulin. Int. J. Biol. Macromol. 50, 1095–1102. https://doi.org/10.1016/j.ijbiomac.2012.03.002.
Murshudov, G.N., Skubák, P., Lebedev, A.A., Pannu, N.S., Steiner, R.A., Nicholls, R.A., Winn, M.D., Long, F., Vagin, A.A., 2011. REFMAC5 for the refinement of macromolecular crystal structures. Acta Crystallogr. D. Biol. Crystallogr. 67, 355–367. https://doi.org/10.1107/S0907444911001314.
Needleman, S.B., Wunsch, C.D., 1970. A general method applicable to the search for similarities in the amino acid sequence of two proteins. J. Mol. Biol. 48, 443–453. https://doi.org/10.1016/0022-2836(70)90057-4.
Pandurangan, A.P., Ochoa-Montaño, B., Ascher, D.B., Blundell, T.L., 2017. SDM: a server for predicting effects of mutations on protein stability. Nucleic Acids Res. 45, W229–W235. https://doi.org/10.1093/nar/gkx439.
Petit, J., Herbig, A.-L., Moreau, A., Delaplace, G., 2011. Influence of calcium on β-lactoglobulin denaturation kinetics: Implications in unfolding and aggregation mechanisms. J. Dairy Sci. 94, 5794–5810. https://doi.org/10.3168/JDS.2011-4470.
Pires, D.E.V., Ascher, D.B., Blundell, T.L., 2014. DUET: a server for predicting effects of mutations on protein stability using an integrated computational approach. Nucleic Acids Res. 42, W314–W319. https://doi.org/10.1093/nar/gku411.
Prlic, A., Bliven, S., Rose, P.W., Bluhm, W.F., Bizon, C., Godzik, A., Bourne, P.E., 2010. Pre-calculated protein structure alignments at the RCSB PDB website. Bioinformatics 26, 2983–2985. https://doi.org/10.1093/bioinformatics/btq572.
Puyol, P., Perez, M.D., Peiro, J.M., Calvo, M., 1994. Effect of binding of retinol and palmitic acid to bovine β-lactoglobulin on its resistance to thermal denaturation. J. Dairy Sci. 77, 1494–1502. https://doi.org/10.3168/jds.S0022-0302(94)77088-0.
Qi, X.L., Brownlow, S., Holt, C., Sellers, P., 1995. Thermal denaturation of β-lactoglobulin: effect of protein concentration at pH 6.75 and 8.05. Biochim. Biophys. Acta - Protein Struct. Mol. Enzymol. 1248, 43–49. https://doi.org/10.1016/0167-4838(94)00225-6.
Qi, X.L., Holt, C., McNulty, D., Clarke, D.T., Brownlow, S., Jones, G.R., 1997. Effect of temperature on the secondary structure of beta-lactoglobulin at pH 6.7, as determined by CD and IR spectroscopy: a test of the molten globule hypothesis. Biochem. J. 324 (Pt 1), 341–346.
Qin, B.Y., Bewley, M.C., Creamer, L.K., Baker, H.M., Baker, E.N., Jameson, G.B., 1998. Structural basis of the Tanford transition of bovine beta-lactoglobulin. Biochemistry 37, 14014–14023. https://doi.org/10.1021/bi981016t.
Read, R.J., Adams, P.D., McCoy, A.J., 2013. Intensity statistics in the presence of translational noncrystallographic symmetry. Acta Crystallogr. Sect. D Biol. Crystallogr. 69, 176–183. https://doi.org/10.1107/S0907444912045374.
Renard, D., Lefebvre, J., Griffin, M.C., Griffin, W., 1998. Effects of pH and salt environment on the association of β-lactoglobulin revealed by intrinsic fluorescence studies. Int. J. Biol. Macromol. 22, 41–49. https://doi.org/10.1016/S0141-8130(97)00086-X.
Richter, A., Eggenstein, E., Skerra, A., 2014. Anticalins: Exploiting a non-Ig scaffold with hypervariable loops for the engineering of binding proteins. FEBS Lett. 588, 213–218. https://doi.org/10.1016/J.FEBSLET.2013.11.006.
Richter, A., Skerra, A., 2017. Anticalins directed against vascular endothelial growth factor receptor 3 (VEGFR-3) with picomolar affinities show potential for medical therapy and in vivo imaging. Biol. Chem. 398, 39–55. https://doi.org/10.1515/hsz-2016-0195.
Rothe, C., Skerra, A., 2018. Anticalin® Proteins as Therapeutic Agents in Human Diseases. BioDrugs 32, 233–243. https://doi.org/10.1007/s40259-018-0278-1.
Rudra, S., Jana, A., Sepay, N., Patel, B.K., Mahapatra, A., 2018. Characterization of the binding of strychnine with bovine β-lactoglobulin and human lysozyme using spectroscopic, kinetic and molecular docking analysis. New J. Chem. 42, 8615–8628. https://doi.org/10.1039/C8NJ00810H.
Sakurai, K., Goto, Y., 2006. Dynamics and mechanism of the Tanford transition of bovine beta-lactoglobulin studied using heteronuclear NMR spectroscopy. J. Mol. Biol. 356, 483–496. https://doi.org/10.1016/j.jmb.2005.11.038.
Sakurai, K., Goto, Y., 2002. Manipulating monomer-dimer equilibrium of bovine Beta -lactoglobulin by amino acid substitution. J. Biol. Chem. 277, 25735–25740. https://doi.org/10.1074/jbc.M203659200.
Sawyer, L., 2013. Advanced Dairy Chemistry. Springer, US, Boston, MA doi: 10.1007/978-1-4614-4714-6.
Shafaei, Z., Ghalandari, B., Vaseghi, A., Divsalar, A., Haertlé, T., Saboury, A.A., Sawyer, L., 2017. β-Lactoglobulin: an efficient nanocarrier for advanced delivery systems. Nanomedicine Nanotechnology. Biol. Med. 13, 1685–1692. https://doi.org/10.1016/J.NANO.2017.03.007.
Shahraki, S., Shiri, F., 2018. Binding interaction of isoxsuprine hydrochloride and levothyroxine to milk β-lactoglobulin; from the perspective of comparison. Int. J. Biol. Macromol. 109, 576–588. https://doi.org/10.1016/J.IJBIOMAC.2017.12.117.
Shepard, H.M., Phillips, G.L.D., Thanos, C., Feldmann, M., 2017. Developments in therapy with monoclonal antibodies and related proteins. Clin. Med. (Northfield. Il). 17, 220–232. https://doi.org/10.7861/clinmedicine.17-3-220.
Skerra, A., 2013. Anticalins: An emerging class of novel biologics to treat cancer and other severe diseases. Drugs Future 38, 169. https://doi.org/10.1358/dof.2013.038.03.1931054.
Taheri-Kafrani, A., Tavakkoli Koupaie, N., Haertlé, T., 2015. β-Lactoglobulin mutant Lys69Asn has attenuated IgE and increased retinol binding activity. J. Biotechnol. 212, 181–188. https://doi.org/10.1016/J.JBIOTEC.2015.08.006.
Taulier, N., Chalikian, T.V., 2001. Characterization of pH-induced transitions of beta-lactoglobulin: ultrasonic, densimetric, and spectroscopic studies. J. Mol. Biol. 314, 873–889. https://doi.org/10.1006/jmbi.2001.5188.
Tumlin, J.A.., 2019. US20190054226A1 - Methods and apparatus for kidney dialysis and extracorporeal detoxification - Google Patents [WWW Document]. United States Pat. Appl. Publ. URL https://patents.google.com/patent/US20190054226A1/en (accessed 12.29.19).
van Stokkum, I.H.M., Laptenok, S.P., 2014. Quantitative Fluorescence Spectral Analysis of Protein Denaturation. pp. 43–51. doi: 10.1007/978-1-62703-649-8_3.
Wang, Q., Allen, J.C., Swaisgood, H.E., 1998. Protein Concentration Dependence of Palmitate Binding to β-Lactoglobulin. J. Dairy Sci. 81, 76–81. https://doi.org/10.3168/jds.S0022-0302(98)75553-5.
Wilde, S.C., Keppler, J.K., Palani, K., Schwarz, K., 2016. β-Lactoglobulin as nano-transporter – Part I: Binding of organosulfur compounds. Food Chem. 197, 1015–1021. https://doi.org/10.1016/J.FOODCHEM.2015.11.010.
Winn, M.D., Ballard, C.C., Cowtan, K.D., Dodson, E.J., Emsley, P., Evans, P.R., Keegan, R.M., Krissinel, E.B., Leslie, A.G.W., McCoy, A., McNicholas, S.J., Murshudov, G.N., Pannu, N.S., Potterton, E.A., Powell, H.R., Read, R.J., Vagin, A., Wilson, K.S., 2011. Overview of the CCP4 suite and current developments. Acta Crystallogr. D. Biol. Crystallogr. 67, 235–242. https://doi.org/10.1107/S0907444910045749.
Wu, X., Lu, Y., Xu, H., Lin, D., He, Z., Wu, H., Liu, L., Wang, Z., 2018. Reducing the allergenic capacity of β-lactoglobulin by covalent conjugation with dietary polyphenols. Food Chem. 256, 427–434. https://doi.org/10.1016/J.FOODCHEM.2018.02.158.
Xia, Y., Chu, W., Qi, Q., Xun, L., 2015. New insights into the QuikChangeTM process guide the use of Phusion DNA polymerase for site-directed mutagenesis. e12–e12. Nucleic Acids Res. 43. https://doi.org/10.1093/nar/gku1189.
Yagi, M., Sakurai, K., Kalidas, C., Batt, C.A., Goto, Y., 2003. Reversible unfolding of bovine beta-lactoglobulin mutants without a free thiol group. J. Biol. Chem. 278, 47009–47015. https://doi.org/10.1074/jbc.M308592200.
Yu, C.-M., Mun, S., Wang, N.-H.L., 2006. Theoretical analysis of the effects of reversible dimerization in size exclusion chromatography. J. Chromatogr. A 1132, 99–108. https://doi.org/10.1016/J.CHROMA.2006.07.017.
Zhao, H.-Y., Feng, H., 2018. Engineering Bacillus pumilus alkaline serine protease to increase its low-temperature proteolytic activity by directed evolution. BMC Biotechnol. 18, 34. https://doi.org/10.1186/s12896-018-0451-0.